REPORT DOCUMENTATION PAGE

Form Approved
OMB No. 0704-0188

Public reporting burden for this collection of information is estimated to average 1 hour per response, including the time for reviewing instructions, searching data sources, gathering and maintaining the data needed, and completing and reviewing the collection of information. Send comments regarding this burden estimate or any other aspect of this collection of information, including suggestions for reducing this burden to Washington Headquarters Service, Directorate for Information Operations and Reports, 1215 Jefferson Davis Highway, Suite 1204, Arlington, VA 22202-4302, and to the Office of Management and Budget, Paperwork Reduction Project (0704-0188) Washington, DC 20503.
PLEASE DO NOT RETURN YOUR FORM TO THE ABOVE ADDRESS.

1. REPORT DATE (DD-MM-YYYY)	2. REPORT TYPE	3. DATES COVERED (From – To)
	Final Technical Report	01 April 2004 – 31 December 2006

4. TITLE AND SUBTITLE
Charge Transfer Nanocomposites: The Effects of Scale-Hierarchy

5a. CONTRACT NUMBER

5b. GRANT NUMBER
FA9550-04-1-0161

5c. PROGRAM ELEMENT NUMBER

6. AUTHOR(S)
Dr. David L. Carroll

5d. PROJECT NUMBER

5e. TASK NUMBER

5f. WORK UNIT NUMBER

7. PERFORMING ORGANIZATION NAME(S) AND ADDRESS(ES
Department of Physics
Wake Forest University
Winston-Salem NC 27109

8. PERFORMING ORGANIZATION REPORT NUMBER

9. SPONSORING/MONITORING AGENCY NAME(S) AND ADDRESS(ES)
Air Force Office of Scientific Research (AFOSR)
875 N. Arlington St., Rm. 3112
Arlington, VA 22203
Dr Charles Lee (WL

10. SPONSOR/MONITOR'S ACRONYM(S)
AFOSR

11. SPONSORING/MONITORING AGENCY REPORT NUMBER
N/A

12. DISTRIBUTION AVAILABILITY STATEMENT
DISTRIBUTION A: Approved for public release. Distribution is unlimited.

AFRL-SR-AR-TR-07-0164

13. SUPPLEMENTARY NOTES

14. ABSTRACT
In this work, we have accomplished the preparation and characterization of the optical properties of 280 nm silica nanospheres coated with a luminescent conjugated polyelectrolyte, sulfonated Poly(phenylene ethynylene) (PPE-SO3-). The conjugated polymer is coated onto the nanospheres by the L-b-L method. Previous shell construction by means of a non-luminescent electrolytic polymer host, blended with luminescent semi-conducting nanocrystals is advanced in this work by constructing the shell from a luminescent polyelectrolyte. Furthermore, we have prepared fluorescent opal structures from these core-shell structures and investigated their optical properties.

15. SUBJECT TERMS

16. SECURITY CLASSIFICATION OF:			17. LIMITATION OF ABSTRACT	18. NUMBER OF PAGES	19a. NAME OF RESPONSIBLE PERSON
a. REPORT	b. ABSTRACT	c. THIS PAGE			19b. TELEPONE NUMBER (*Include area code*)
Unclassified	Unclassified	Unclassified	Unclassified	45	(703)

Final report • FA9550-04-1-0161 • Charge Transfer Nanocomposites: the effects of scale hierarchy

Investigator: Dr. David L. Carroll
Dept. of Physics
Wake Forest University
Winston-Salem NC 27109
Ph. (336) 768 5508
Email: carroldl@wfu.edu

Performing Institution:
The Center for Nanotechnology and Molecular Materials
Wake Forest University
Winston-Salem NC 27109

AFOSR POC: Charles Y-C Lee, Ph. D.
AFOSR/NL
4015 Wilson Blvd, Room 713
Arlington, VA 22203-1954
Phone: (703) 696-7779
Fax: (703) 696-8449
Email: charles.lee@afosr.af.mil

Performance Period: 01/15/04 – 01/01/07

1.0 PROGRAM OBJECTIVES

(1) The program will quantify charge transfer mechanisms and relevant time scales associated with nanoparticulate / electro-active polymer blends (Charge transfer nanocomposites). These will be correlated with induced morphological modifications, modifications to optical absorption cross-sections, and effects of localization.
(2) The program will then examine electronic and optical phenomena associated with degrees of matrix order/disorder, or "Scale-Hierarchy", in the nanocomposites. We will address the question: "when the nano-particles are ordered over length scales that are commensurate with polarons/excitons or wavelength of incident light, are nanotube-host interactions modified"
(3) Finally, the program will integrate nanotube-based matrix composites into organic photovoltaic devices and organic optical sensing devices (CCDs and photodiodes).

2.0 DELIVERABLES

The program will focus on *nanotube* - polymer interactions and how these they might be modified when the nanotubes are ordered within the matrix.

I. A systematic study of charge transfer phenomena (energy levels/times/majority carrier/etc.) between nanotubes and conjugated polymer hosts will be made. Varied host materials, PPVs (MEH-PPV, DOO-PPV, PmPV, POMPV), PFO (Dow Chemical), P3OT, PANI, PEDOT will allow correlation with host bulk properties.

II. X-ray, dynamic light scattering, microscopy (confocal, SEM, TEM, STM, NSOM), Raman and micro-Raman will determine the order parameters for heavily loaded composites. Three "dimensions of order" in the nanodispersant matrix will be considered for thin films: (1) Random matrix, (2) Fractal structures, (3) Aligned structures in 2-D.

III. The coupling between incident radiation and electronic response of these systems will be determined as a function of the meso-scale structure built into the dispersion. Photoluminescence lifetime, electroluminescence efficiencies, optically stimulated time-of-flight (TOF) as well as pump-probe experiments on the nano-second and pico-second time frames will be the mainstay of experimentation. Modeling of the field within the composite layers will be used to understand how absorption cross-sections are modified.

IV. Organic photovoltaics and optical detection pixels (photodiodes) for integration into CCDs will be used as test beds for the nanocomposites. Each of these devices present unique opportunities for advancement in state-of-the-art using nanocomposites.

This report lists only the major advances of the program and is NOT exhaustive.

3.0 SUMMARY STATEMENT

In considering a nanocomposite material composed of electrically and optically active nanomaterials dispersed within an electrically and optically active host material, three fundamental interactions must define and determine the overall optical and electronic properties of the composite. They are;

I. Energy transfer and partitioning within the nanophase
II. Energy transfer and partitioning within the host
III. Energy transfer and partitioning between host and nanophase

Each of these represents optical as well as electronic energy transfer, in triplet or singlet excitations, and thus they are quite broad in their overall implications. Each of these is intimately dependent on the local ordering of host and nanophase, as well as the meso-ordering of host and nanophase. And, each of these, self-consistently influences the others.

The *ansatz* of this program has been 1) a study of the effects of how local and meso-scale ordering (scale hierarchy) might influence these fundamental mechanisms for determining nanocomposite behavior. 2) We have also provided a demonstration of how this helps us in the design and fabrication of novel new organic photonic technologies such as photovoltaics.

Figure 3.1: A model of Electro-Active Nanocomposites

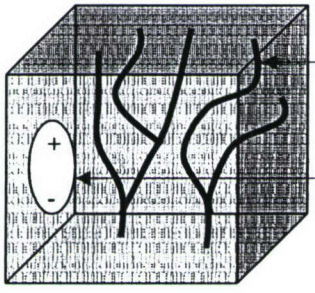

The symmetry and structure of the nanophase over the scale of nanometers to microns, determines its overall oscillator strength (antenna properties)

The oscillator strength of the nanophase determines the interactions with charged excitons

Thus when placing and antenna into the exciton meliu of the host, how good of an antenna is used determines overall energy transfer dynamics.

This report lists only the major advances of the program and is NOT exhaustive.

4.0 PROGRAM RESULTS: Scientific

4.1 *Photonic Three Dimensional Assemblies*

The simplest and most obvious approach to the creation of 3_D assemblies in a polymer host, is the intercalation of active polymers host into a photonic band gap structure. The interesting aspect of this approach is that the oscillator strength of such as system is very small. Thus, modification to propagating-modes in the system can be studied outside of the effects of the charged interactions. References and an introduction have been included in this section.

Description

Considerable attention has been drawn to photonic crystals of self-assembled colloidal nano- and micro- sized spheres due to their interesting optical properties in the visible and near infrared wavelengths respectively.[1-8] An active material placed within a photonic crystal that has a radiative transition inside the photonic band gap (PBG) formed by these structures will be unable to emit a photon, and will result in the formation of a *photon-atom* bound state.[9] This should lead to interesting quantum phenomena such as two and three dimensional photonic band-gap lasers. [10, 11] Localized and extended defects can then be engineered in the PGB to produce high-Q microcavities and waveguides.[12,13]

Selective and precise modification of the optical properties of photonic crystal colloidal arrays by applying various coatings to the spheres is attractive for building multipurpose structures and devices. Previously, the most common luminescent hybrid photonic colloidal structures have been constructed by infiltrating emissive polymers, polymer blends containing laser dyes, and semi-conducting nanocrystals into the voids of these structures.[3, 14-18] Inverse photonic structures with luminescent polymer templates have also been synthesized by infiltration techniques and have been composed of various materials.[19] The optical quality of these previously mentioned structures is dependent upon maintaining an isotropic steric packing of the spheres and ensuring a homogenous distribution of the filling polymer or oligomer. A distinct disadvantage to the infiltration method is the inherent disruption or unpacking of these structures during infiltration and/or polymerization leading to decreased optical performance.[15]

To avoid difficulties resulting from the disruptive infiltration method, Rogach et al. [16] have engineered a core-shell structure by pre-coating the spheres with a polymer – luminescent semi-conducting nanocrystalline composite. Their shell structure was deposited by the Layer-by-Layer (L-b-L) process, where electrostatic forces between polycationic and polyanionic species drive self-assembly into monodispersive layers.[20-22] L-b-L construction of core-shell photonic colloids offers control of the shell thickness on the order of nanometers, allowing for the precise tuning of the pseudo-photonic band gap or stop band, and adding the functionality of the specific polyelectrolyte while maintaining high quality photonic structures.

Final report • FA9550-04-1-0161 • Charge Transfer Nanocomposites: the effects of scale hierarchy

In this work, we have accomplished the preparation and characterization of the optical properties of 280 nm silica nanospheres coated with a luminescent conjugated polyelectrolyte, sulfonated Poly(phenylene ethynylene) (PPE-SO3-).[23] The conjugated polymer is coated onto the nanospheres by the L-b-L method. Previous shell construction by means of a non-luminescent electrolytic polymer host, blended with luminescent semi-conducting nanocrystals is advanced in this work by constructing the shell from a luminescent polyelectrolyte. Furthermore, we have prepared fluorescent opal structures from these core-shell structures and investigated their optical properties.

The PPE was provided by Kirk Schanze at the University of Florida. The main results are shown here and have been submitted for publication to *Advanced Materials*:

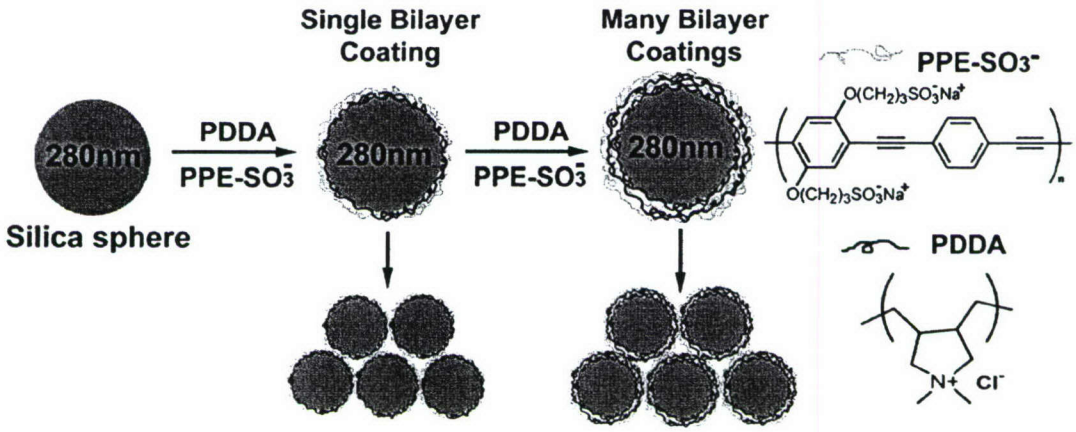

Scheme 4.1. Layer-by-Layer construction of PDDA/PPE-SO3- bilayer coated silica spheres and the structures of PPE-SO3- and PDDA.

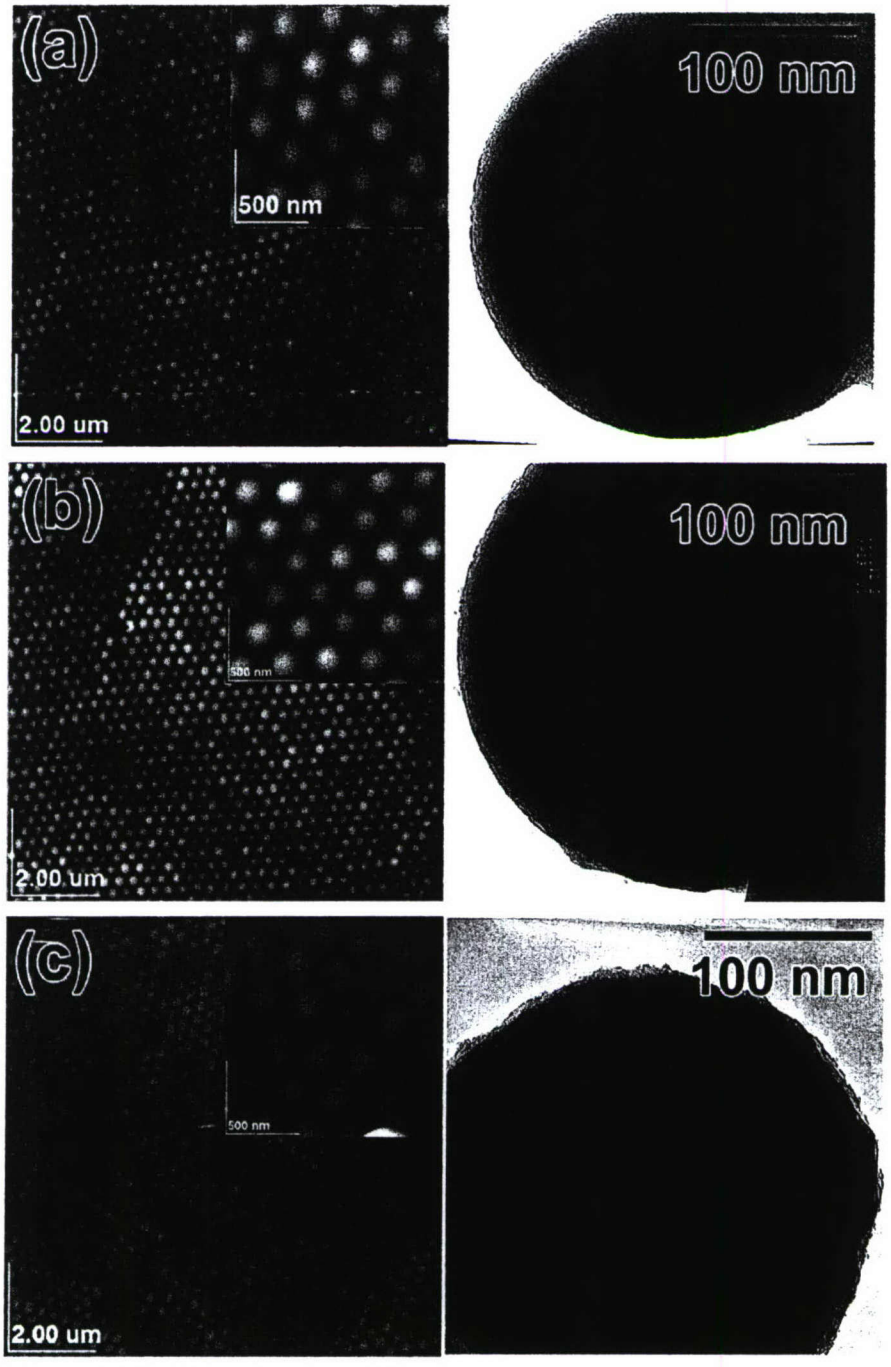

Figure 4.1. AFM images of the thin film photonic crystals and TEM micrographs of the constituent spheres (a) uncoated, (b)1 bilayer, and (c) 5 bilayer coatings.

This report lists only the major advances of the program and is NOT exhaustive.

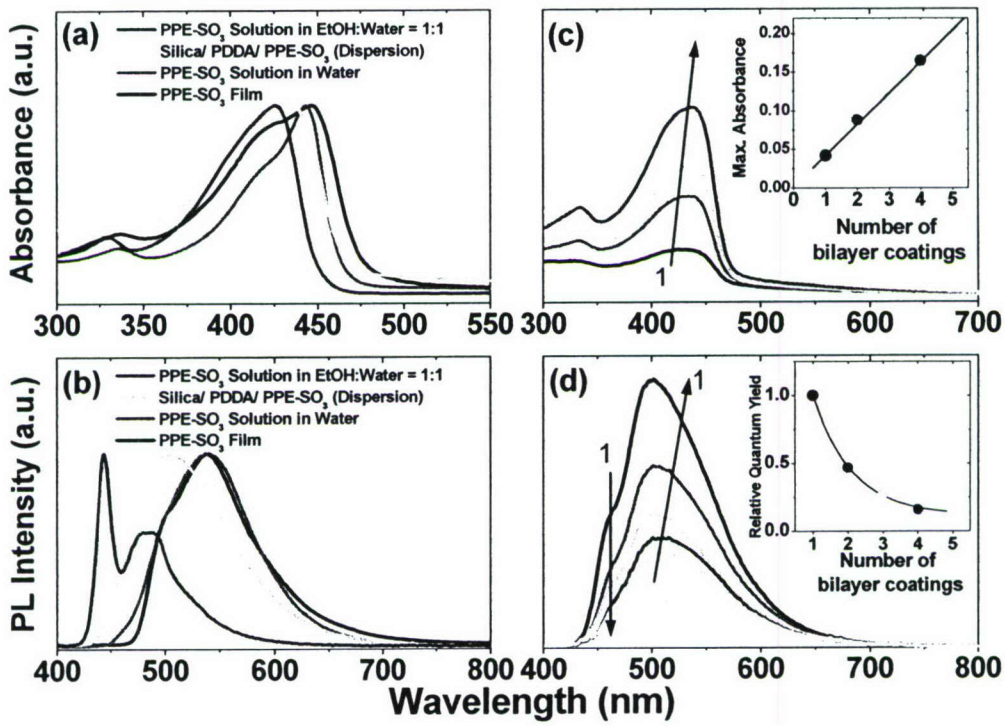

Figure 4.2. (a) Absorption and (b) photoluminescence spectra of PPE-SO3- morphologies increasing from non-aggregated (Blue) to aggregated (Black). (c) Absorption and (d) photoluminescence spectra of (PPE-SO3-/PDDA)n/Silica colloidal suspensions in ethanol with increasing bilayer concentration from n equal to 1 (Black) to 5 (Cyan). Inset (c) is the linear fit to the absorption maximum in Figure 1(c) at 425 nm. Inset (d) is an exponential fit to the decreasing quantum yield in Figure 1(d) at 500 nm.

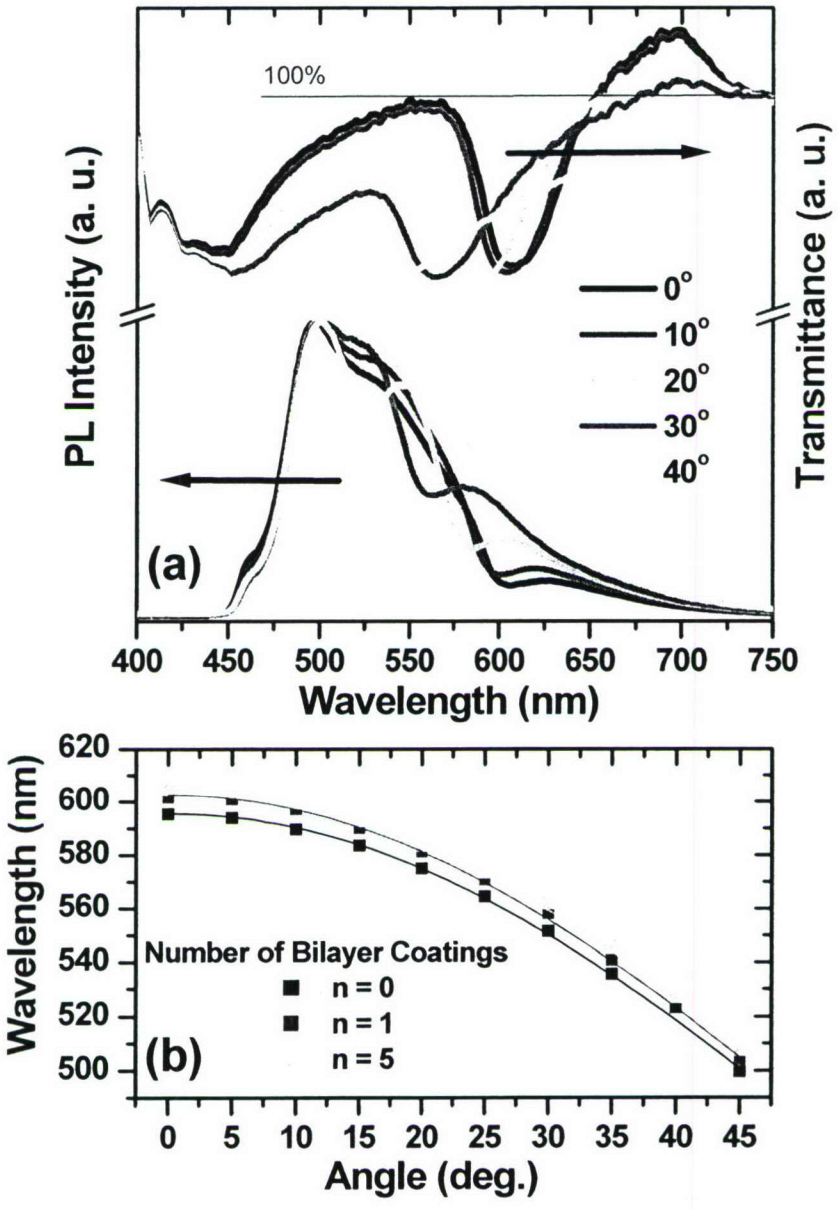

Figure 4.3. (a) Angle dependent transmission (Right) and photoluminescence (Left) of a typical thin film photonic crystals with 5 bilayers from 0 to 40 degrees. (b) Fitted maximum stop band wavelength verses angle for several bilayer coatings.

Summary

In Summary, this experiment clearly demonstrates that final state effects 9that is the allowed propagating modes of the system, influence exciton recombination dynamics without ay direct charged interactions with the excitons themselves. In the context of these studies this is important since it points out that the overall structure of the meso-phase is important in determining such effects without any antenna interactions at all!

References

[1] H. Fudouzi, Y. N. Xia, *Adv Mater* **2003**, *15*, 892.
[2] H. Miguez, S. M. Yang, N. Tetreault, G. A. Ozin, *Adv Mater* **2002**, *14*, 1805.
[3] R. C. Polson, A. Chipouline, Z. V. Vardeny, *Adv Mater* **2001**, *13*, 760.
[4] H. Miguez, C. Lopez, F. Meseguer, A. Blanco, L. Vazquez, R. Mayoral, M. Ocana, V. Fornes, A. Mifsud, *Appl. Phys. Lett.* **1997**, *71*, 1148.
[5] K. Sumioka, H. Nagahama, T. Tsutsui, *Appl. Phys. Lett.* **2001**, *78*, 1328.
[6] W. Wang, B. Gu, L. Liang, W. Hamilton, *J. Phys. Chem. B* **2003**, *107*, 3400.
[7] T. B. Xu, Z. Y. Cheng, Q. M. Zhang, R. H. Baughman, C. Cui, A. A. Zakhidov, J. Su, *J. Appl. Phys.* **2000**, *88*, 405.
[8] I. Luzinov, D. Julthongpiput, A. Liebmann-Vinson, T. Cregger, M. D. Foster, V. V. Tsukruk, *Langmuir* **2000**, *16*, 504.
[9] S. John and J. Wang, Phys. Rev. B 43, **1991** 12772
[10] O. Painter, R. K. Lee, A. Scherer, A. Yariv, J. D. O'Brien, P. D. Dapkus, *Science* **1999**, *284*, 1819.
[11] A. Jebali, R. Harbers, D. Erni, W. Bächtold, R. F. Mahrt, N. Moll, G.-L. Bona, C. Bauer, and E. B. Kley. In *27th Workshop on Compound Semiconductor Devices and Integrated Circuits (WOCSDICE'03)*, pages 83-84. ETH Zürich, 2003.
[12] H. G. Park, J. K. Hwang, J. Huh, H. Y. Ryu, Y. H. Lee, and J. S. Kim, Appl. Phys. Lett. 79, **2001**, 3032.
[13] A. Sugitatsu, T. Asano, and S. Noda Appl. Phys. Lett. 84(26) **2004**, 5395.
[14] M. Deutsch, Y. A. Vlasov, D. J. Norris, *Adv Mater* **2000**, *12*, 1176.
[15] D. J. Norris, Y. A. Vlasov, *Adv Mater* **2001**, *13*, 371.
[16] A. Rogach, A. Susha, F. Caruso, G. Sukhorukov, A. Kornowski, S. Kershaw, H. Mohwald, A. Eychmuller, H. Weller, *Adv Mater* **2000**, *12*, 333.
[17] S. G. Romanov, T. Maka, C. M. S. Torres, M. Muller, R. Zentel, *Appl. Phys. Lett.* **1999**, *75*, 1057.
[18] K. Yoshino, S. Tatsuhara, Y. Kawagishi, M. Ozaki, A. A. Zakhidov, Z. V. Vardeny, *Appl. Phys. Lett.* **1999**, *74*, 2590.
[19] A. Blanco, E. Chomski, S. Grabtchak, M. Ibisate, S. John, S. W. Leonard, C. Lopez, F. Meseguer, H. Miguez, J. P. Mondia, G. A. Ozin, O. Toader, and H. M. van Driel, *Nature* **2000**, *405*, 437.
[20] G. Decher, *Science* **1997**, *277*, 1232.
[21] F. Caruso, *Adv Mater* **2001**, *13*, 11.
[22] D. B. Shenoy, A. A. Antipov, G. B. Sukhorukov, H. Mohwald, *Biomacromolecules* **2003**, *4*, 265.
[23] C. Y. Tan, M. R. Pinto, K. S. Schanze, *Chem Commun* **2002**, 446.

This report lists only the major advances of the program and is NOT exhaustive.

4.2 Electrochromics

Of course when the regular order is removed in the system above, the overall optics is dominated by turbid scatter as would be expected. However, when the individual nanoparticles of the meso-phase have a well defined oscillator strengths (as in the case of plasmonic particles), both near and far field interactions within that nanocomposite dispersion can be observed. This is the case when looking at electrochromism in the host. In this case both charge exchange to the particle from the excitations, and meso-scale dielectric interactions come into play. Specifically, we have shown that the meso-scale dispersion of particles modifies the local dielectric, yielding a shift in the plasmonic bands of the nanophase, and the mobility of excitons are also shifted due to local trapping effects.

Description

To make this demonstration, electrochromic devices were made using a nanocomposite blend of conducting polymer poly(3,4 ethylenedioxythiophene): poly styrene sulfonate (PEDOT:PSS) and metal nanoparticles of silver or gold. Microscopic analysis showed a random distribution of metal nanoparticles with little aggregation in the matrix. The two terminal devices exhibited an increase in absorption that is dependant on the loading of nanoparticles in the polymer. Further, the active electrochromic spectral window showed a bias dependant tuning and a broadened spectral response. All devices exhibited slow relaxivities which we interpret as resulting from the high capacitance of the metal nanoparticles embedded in the polymer matrix.

Results

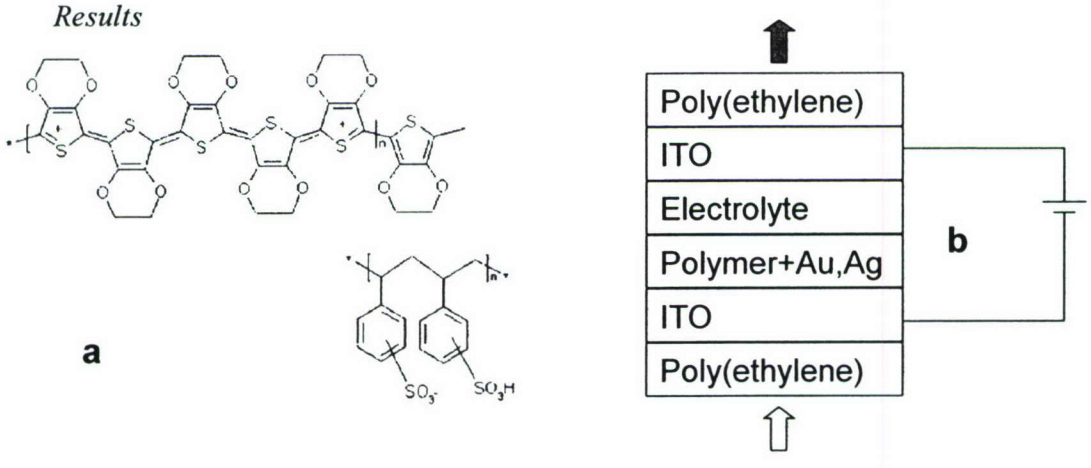

Figure 4.4. a) Chemical structure of PEDOT: PSS, b). The schematic of the electrochromic device structure

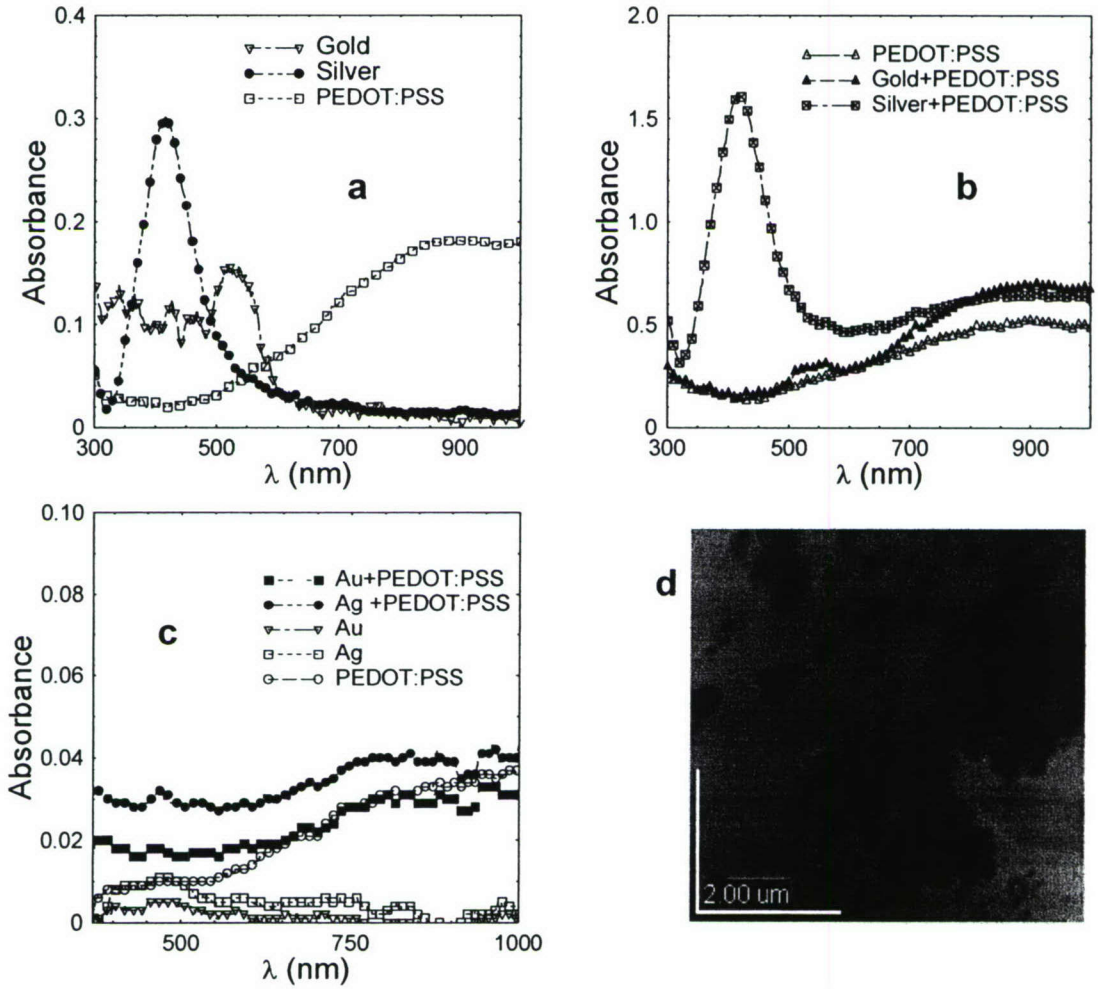

Figure 4.5. a). The absorbance spectrum of dispersion of gold, silver nanoparticles and PEDOT:PSS in water. b) The absorbance spectra of composites mixed in 1:1 ratio of metal nanoparticles dispersion and PEDOT:PSS dispersion. c). The comparison of absorbance spectra of individual thin films and composites thin films. d). AFM (noncontact mode) image of the Au thin film on mica

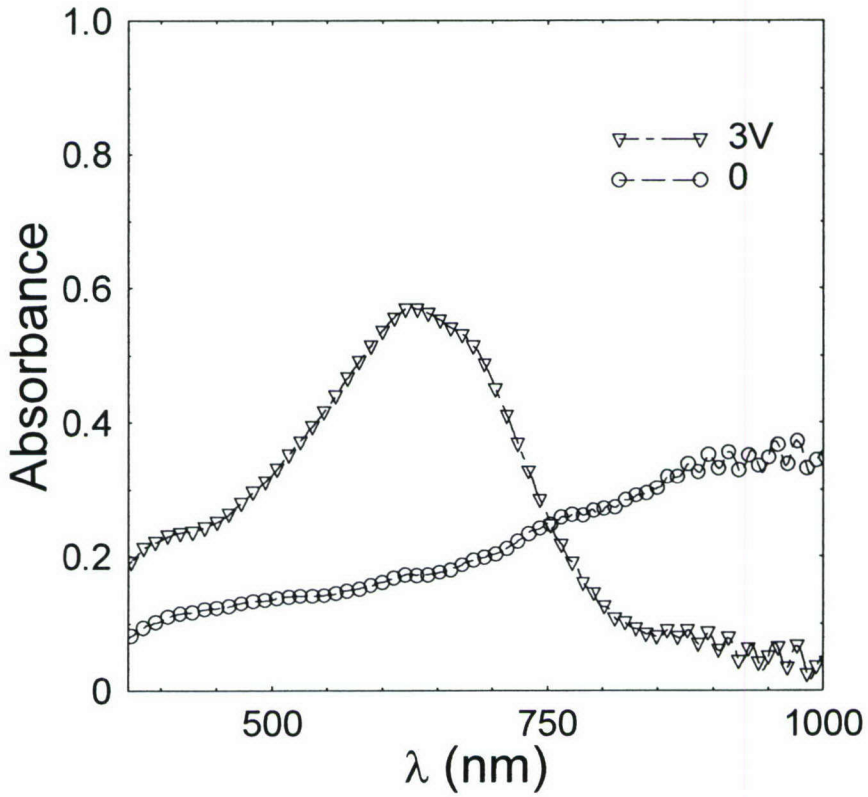

Figure 4.6, The absorbance spectra of the PEDOT: PSS only electrochromic device in different bias conditions

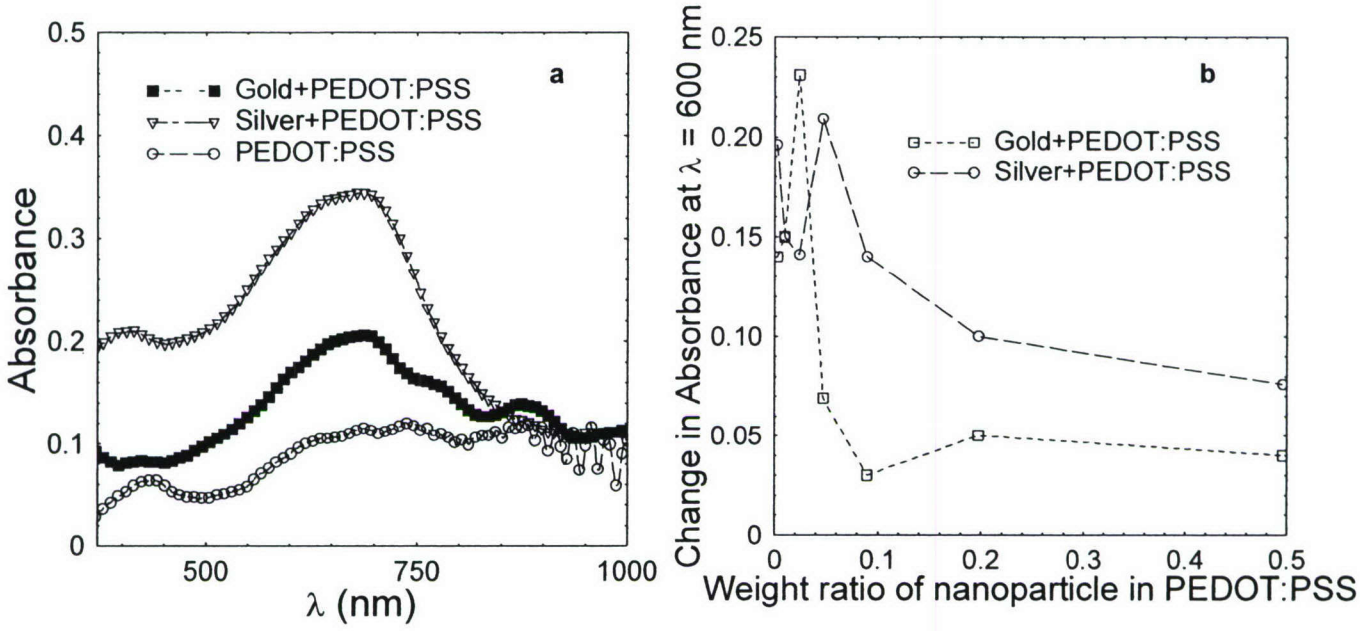

Figure 4.7. a). The electrochromic properties pf the composite b). The absorbance change of the composite device with respect to different loading ratio of the nanoparticles in PEDOT: PSS

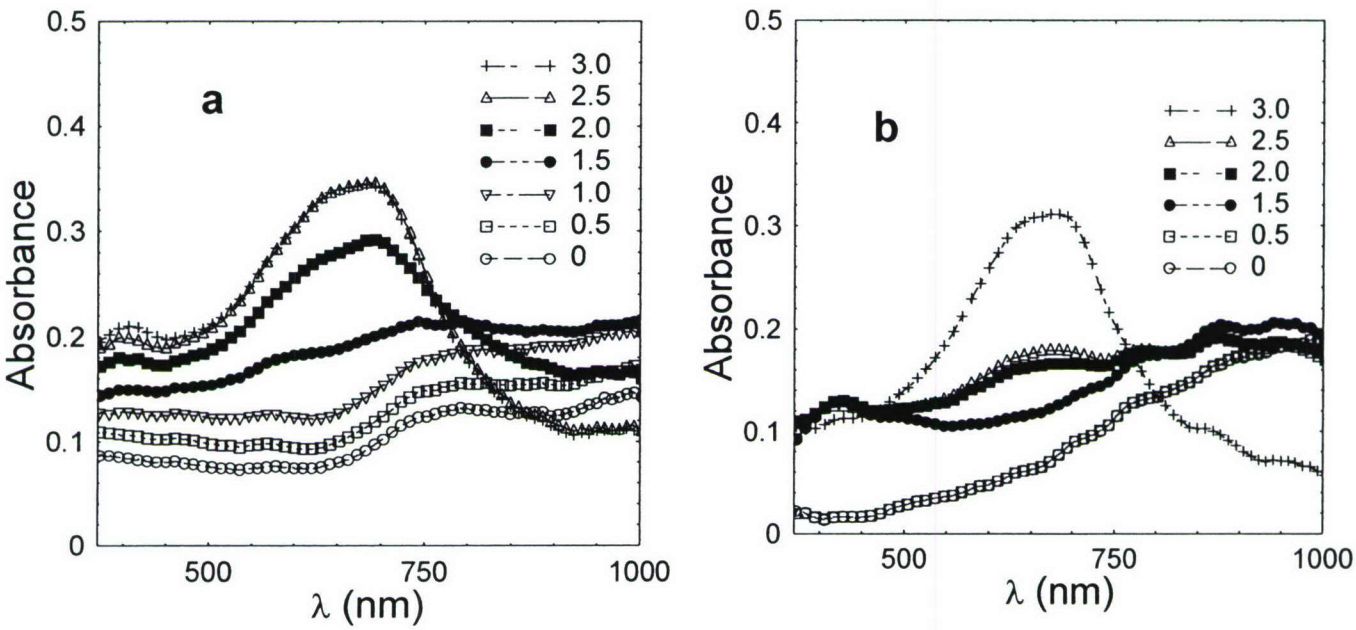

Figure 4.8. a) The bias dependant electrochromic properties of Ag+ PEDOT:PSS composite and b) that of Au+ PEDOT:PSS

This report lists only the major advances of the program and is NOT exhaustive.

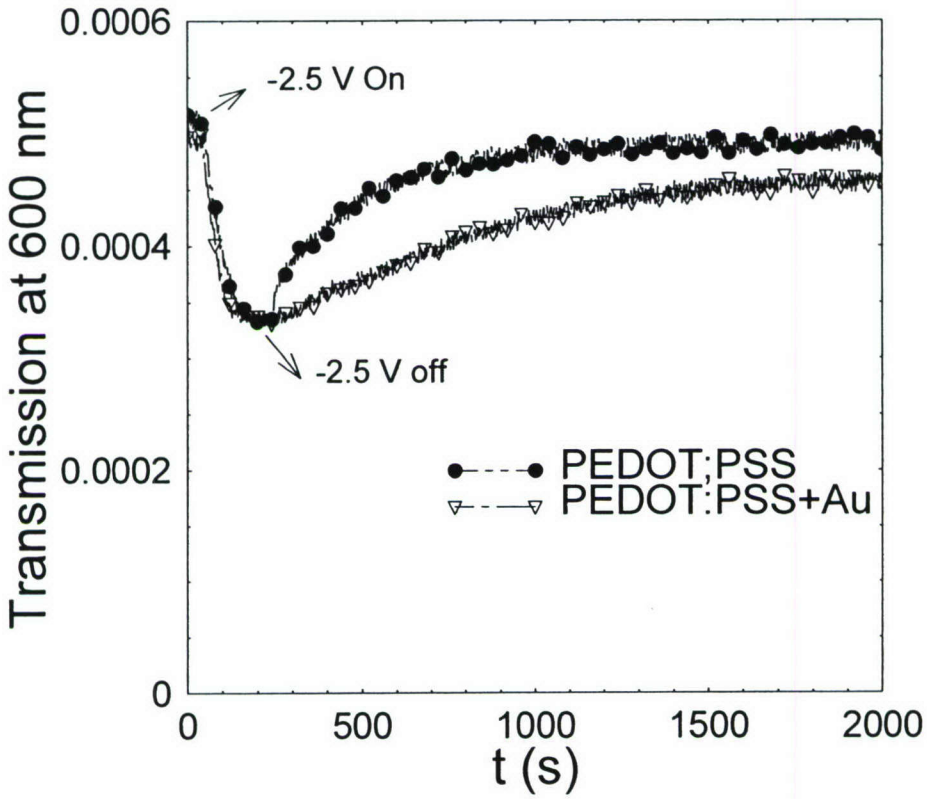

Figure 4.9. The time response of the electrochromc device with respect to voltage ON and OFF state

Summary

Electrochromic devices with nanocomposite blends consisting of metal nanoparticles and conducting polymers were made. The devices showed enhanced absorbance due to plasmon absorption in the nanoparticles. The absorbance enhancement depends on the loading of the nanoparticles in PEDOT: PSS as expected. However, the plasmon absorption peak depends on the dielectric properties of the surrounding medium allowing tuning of the spectral response with voltage. The color tuning and time response makes this material a prospective candidate for full color electrochromic displays.

4.3 Is the Nanotube a Giant Oscillator Strength Material?

An interesting and instructive question investigated in this program has been how important is the oscillator strength of the nanoparticle and do carbon nanotubes couple well (as antennae) to the optical field. This question has been definitively answered in a series of important demonstrations involving phase-coherent absorption effects.

Description

Using nonlinear absorption at 532 nm in the nanosecond regime, we have measured the low fluence nonlinear optical properties of the reverse saturable carbocyanine dye, 1,1',3,3,3',3'-hexamethylindotricarbocyanine iodide (HITCI), blended with well dispersed carbon nanotubes. The nonlinear optical properties of the blend are strongly dependent on the ratio of dye to nanotubes in solution. In the case where the nanotubes per dye molecule ratio is large, we see a distinctive enhancement in optical fluence limiting properties of the system, suggesting enhanced absorption of the excited state manifolds. However, when the nanotube to dye ratio drops, the system response is dominated by the dye's behavior. We suggest that this can be seen as a two component system in which sensitized dye molecules associated with the nanotubes have a different optical cross-section from the dye molecules far from the nanotubes. From classical antennae considerations, this is expected.

Results

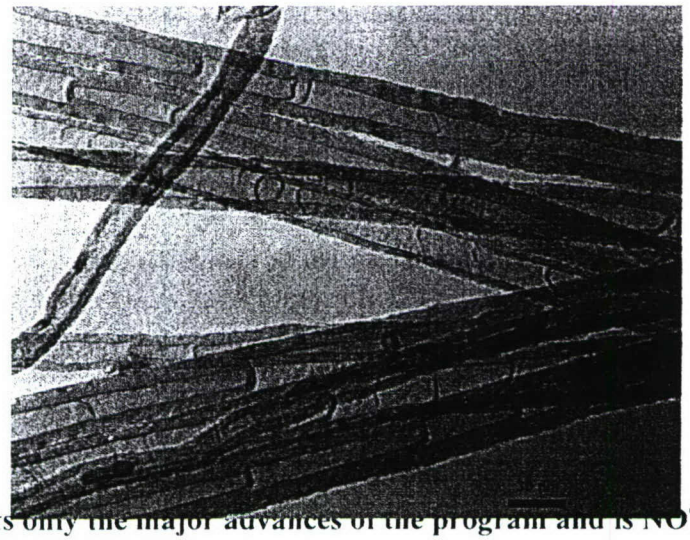

This report lists only the major advances of the program and is NOT exhaustive.

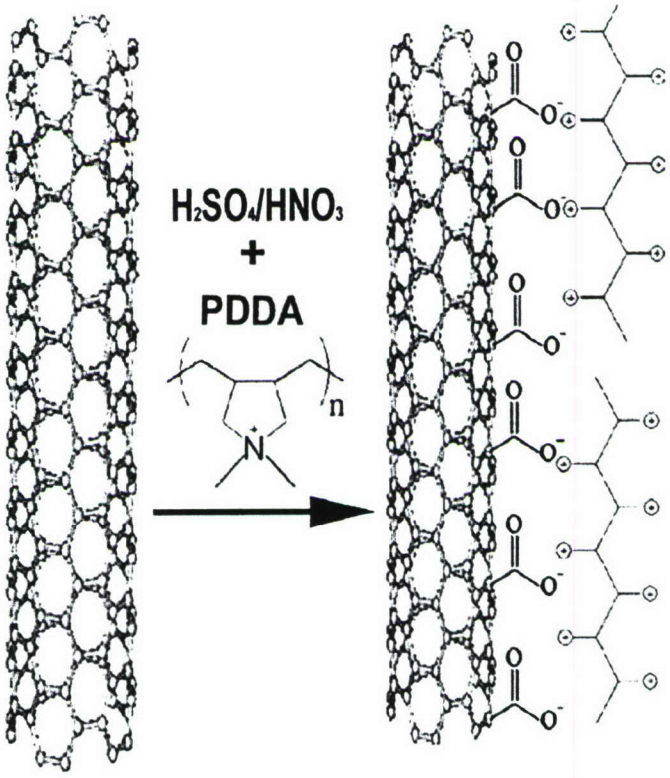

Figure 4.10 TEM of CN_x-MWNTs and functionalization scheme of $PDDA^+CN_x^-$-MWNTs by acid treatment and compatibilization for methanol by electrostatically adsorbed cationic PDDA.

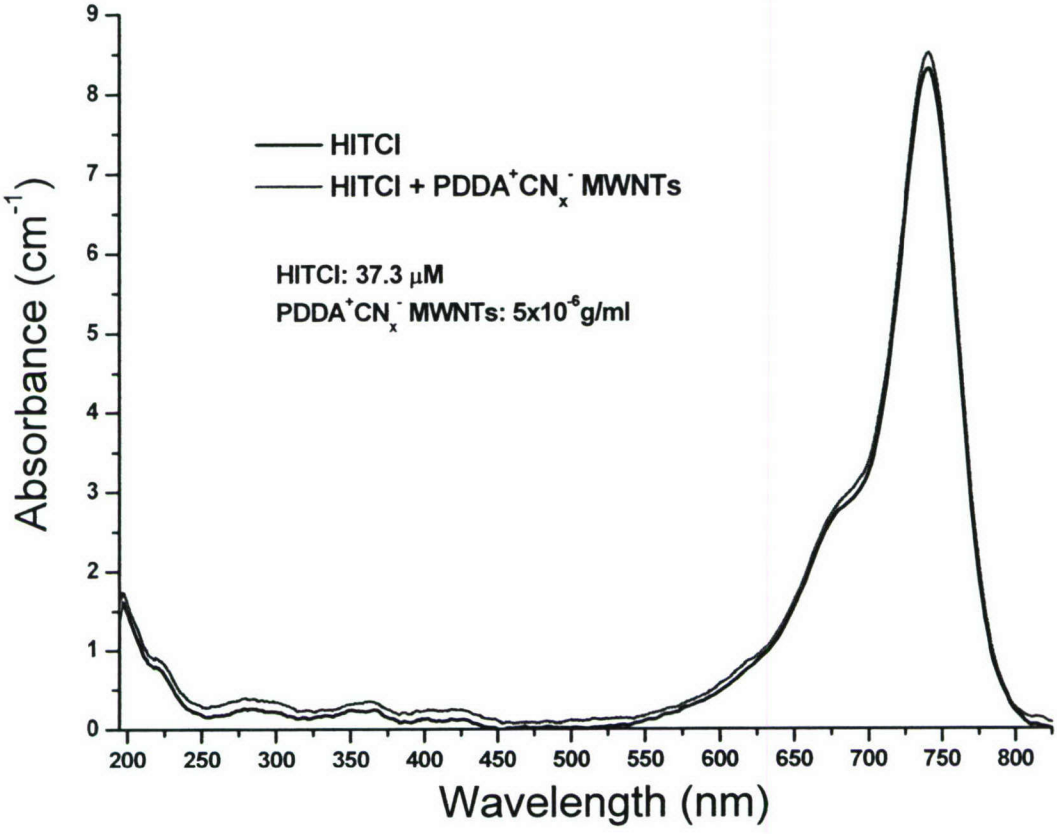

Figure 4.11 Absorbance of HITCl blended with and without with $PDDA^{+}CN_{x}^{-}$-MWNTs. At these low fluences, there is almost no difference in absorption cross-section.

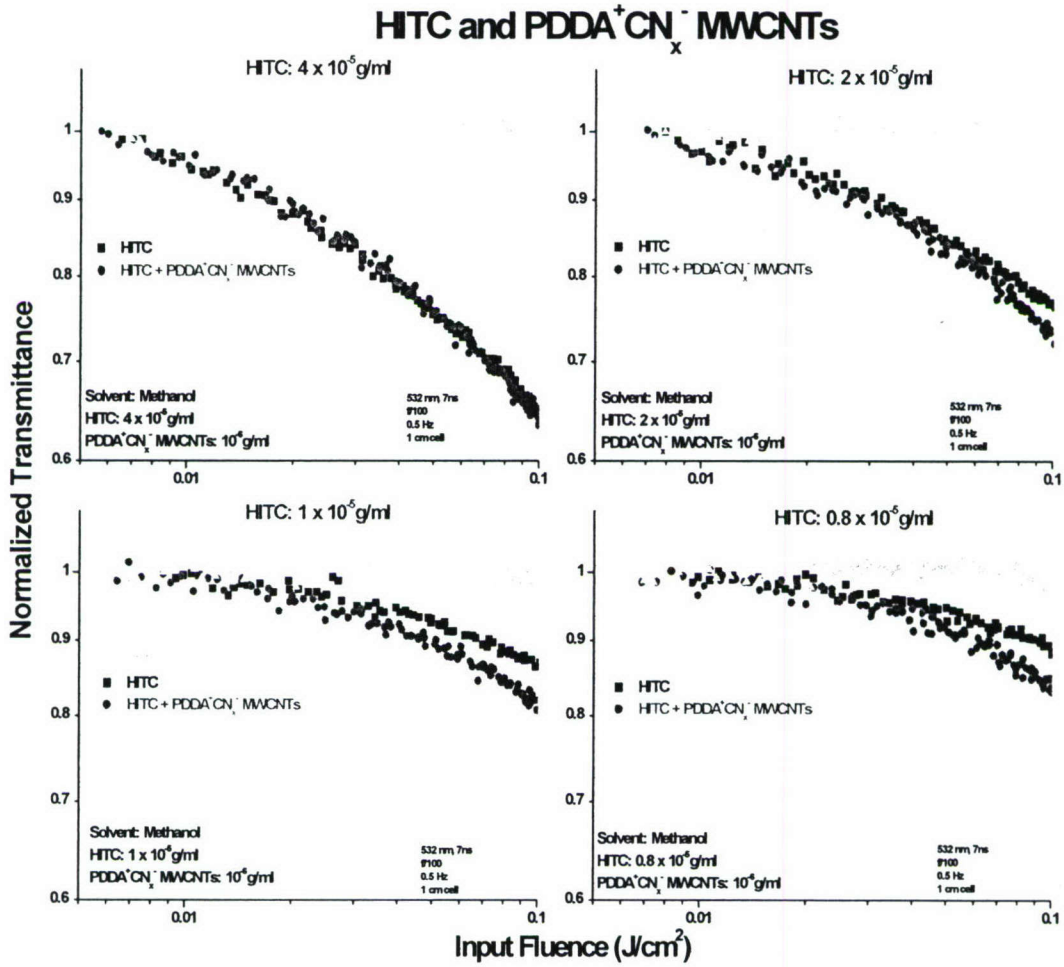

Figure 4.12 Normalized nonlinear transmission spectra at 532 nm of $PDDA^{+}CN_{X}^{-}$-MWNTs (green), HITCI (black), and blended HITCI and $PDDA^{+}CN_{X}^{-}$-MWNTs (red) at molar concentrations of HITCI (a) 74.5 μM, (b) 37.3 μM, (c) 18.6 μM, and (d) 14.9 μM. $PDDA^{+}CN_{X}^{-}$-MWNTs concentration is fixed at $5x10^{-6}$ g/ml. Notice that as the fluence is raised, the presence of the nanotubes clearly enhances the ability of the dye to absorb the light! This is a standard property associated with antenna-mediated phase coherent absorption.

This report lists only the major advances of the program and is NOT exhaustive.

Summary

In summary, nitrogen doped carbon nanotubes were functionalized for compatibilization in methanol and blended with HITCI. The linear properties of the suspensions are only slightly modified by the presence of the nanotubes as an increase in scattering. However, the addition of carbon nanotubes greatly influenced the nonlinear transmittance at low fluences. We suggest that the HITCI's RSA properties at low fluences are modified through "antenna-like" effects by the blended carbon nanotubes.

A useful device made from these blends

Passive nonlinear transmission devices designed to protect sensitive optical components and eyes from laser induced damage are of great interest for military, law enforcement, and industrial applications. An ideal passive nonlinear transmission protective device would respond instantaneously to short picosecond pulses as well as to continuous irradiation. It would have a broadband spectral response without damage and have nearly perfect linear transmission properties. Finally, it would be tailorable to pin the output to a predetermined fluence. To date, most research has been aimed at three classes of passive *limiting* mechanisms with limited success in creating an ideal nonlinear transmission device: (1) multi-photon absorption, (2) reverse saturable absorption (RSA), (3) and nonlinear scattering. Comparatively, little research has been performed using combinations of these mechanisms. Optically engineered solutions of cascaded cells and multipass geometries have shown promising results, but may prove unattractive due to their large physical dimensions.[1,2] Recently, N. Izard et al. [3] reported combining a multi-photon absorber dye with nonlinearly scattering carbon nanotubes to show modest improvements in the blends when studied under optimized focal conditions.

In this work, we have prepared a nonlinear scattering system blended with a RSA dye for complimentary (and additive) nonlinear transmission. Specifically, nitrogen doped multiwalled carbon nanotubes (CN_x-MWNTs) were functionalized for compatibilization in alcohols and blended with a well studied carbocyanine dye, 1,1',3,3,3',3'-hexamethylindotricarbocyanine iodide (HITCI) to investigate the composite system's nonlinear optical response.

---

1. F. E. Hernández, S. Yang, E.W. Van Stryland, and D. J. Hagan, *Optics Letters* **2000**, 25(16), 1180.
2. N. M. Barbosa Neto, C. R. Mendonca, L. Misoguti, and S. C. Zilio, *Optics Letter* **2003**, 28(3), 191
3. N. Izard, C. Ménard, D. Riehl, E. Doris, C. Mioskowski, and E. Anglart, *Chem. Phys. Lett.* **2004**, 391, 124.

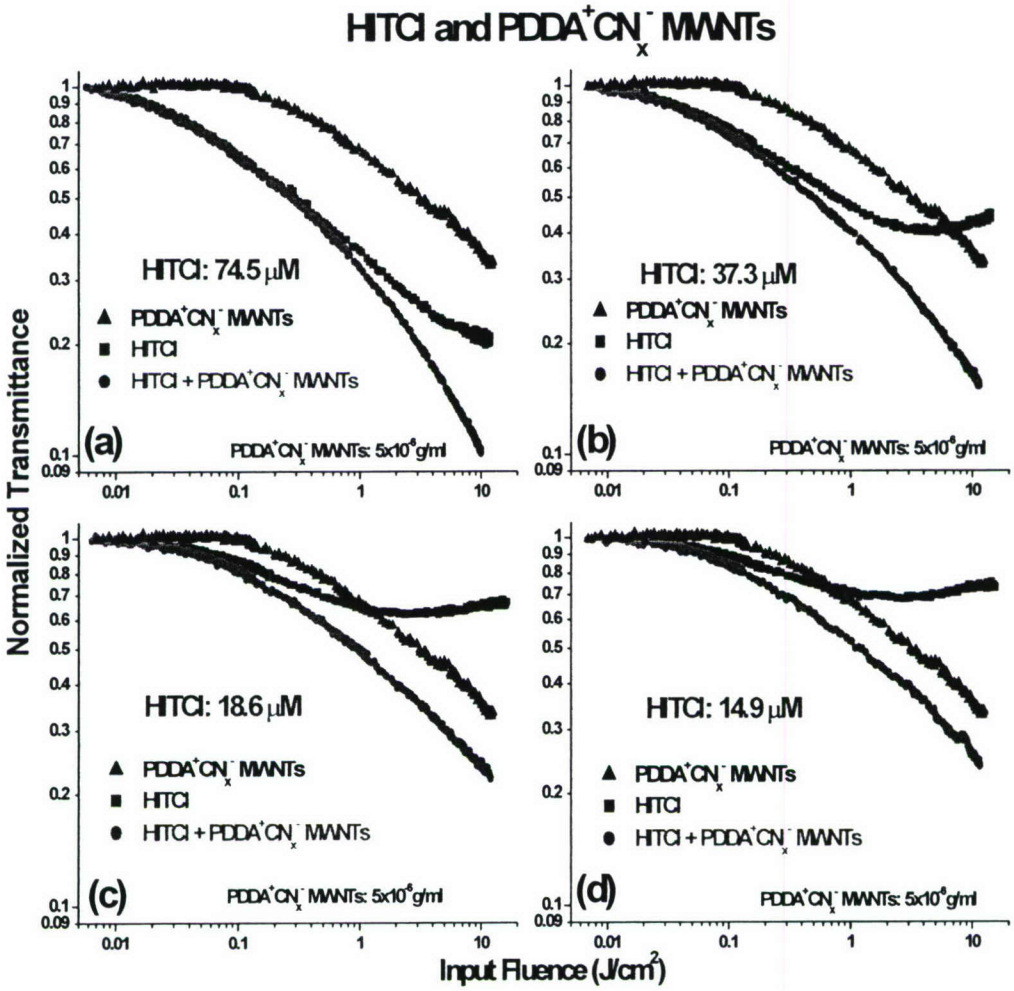

Figure 4.13 Nonlinear transmission spectra at 532 nm of $PDDA^{+}CN_x^{-}$-MWNTs (black), HITCI (blue), and blended HITCI and $PDDA^{+}CN_x^{-}$-MWNTs (red) at molar concentrations of HITCI (a) 74.5 μM, (b) 37.3 μM, (c) 18.6 μM, and (d) 14.9 μM. $PDDA^{+}CN_x^{-}$-MWNTs concentration is fixed at $5x10^{-6}$ g/ml.

4.4 Using the *Giant Oscillator* to explain triplet population lifetime modifications

The fact that organic devices can have greatly extended lifetimes when using nanophase materials such as carbon nanotubes has been established in our previous program and we continue to develop long-lifetime, robust organic electronics using this approach. The question remains: "why?" We have hypothesized that this is due to a modification of triplet lifetimes in the host materials, leading to a suppression of oxidation in the host.

Description

In this program a preliminary investigation of effects on triplet population lifetimes, due to modifications in the nanophase have been undertaken. Specifically, direct measurements of the triplet population lifetimes have been made using time dependent luminescence decay and transient photo-absorption. This preliminary data on the decay of triplet excitons in MEH-PPV loading with carbon nanotubes is shown below and indicates the decreasing lifetime of the triplet exciton as a function of nanotube loading. Note that lifetimes decrease by a factor of 4 for this system, yet we do not know how ordering the nanophase, changing its electronics or modifying its oscillator strength might effect this trend. To test our hypothesis above, each of these variables are currently being varied in a systematic way. Oscillator strength will be varied by changing the length of the nanotubes/nanowires and their loading. Doping the nanotubes will allow us to move its relative position to the HOMO-LUMO band edges of the polymer. And structuring the composite (as described below) can provide insight into how long-range order might effect interactions between nano-antenna and excitons. These studies are ongoing at the end of this program.

Data

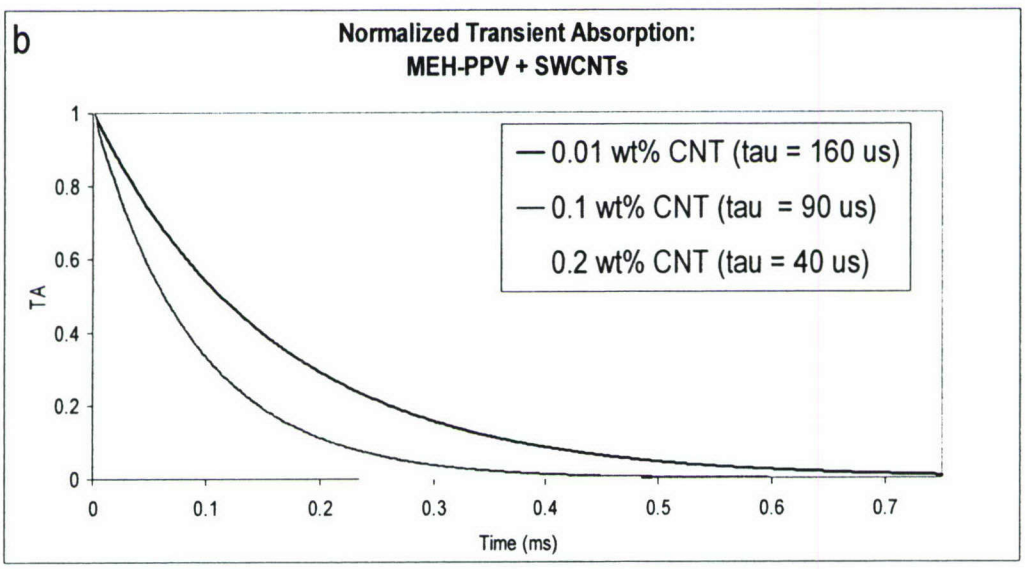

Figure 4.14. Preliminary data on triplet population in MEH-PPV with varying amounts of CNTs. These experiments were carried out at 15K.

Summary

So what do these measurements have to do with the oscillator strength? We know that the triplet state of the polymer is mixed generally speaking: triplet state = (a ψ_T + b ψ_S) and Förster transfer is small because b is small. However: the rate of energy transfer from such state through the Förster mechanism is: $R_F \sim b^2 f_D f_A$. So while $b^2 < a^2$ by about 10^5 , f_A can be increased by about 10^5 because of phase coherence in the nano-particle. Thus, we believe that these experiments show that the triplet lifetime (and thus polymer oxidation time scales) are directly tied to the oscillator strength per unit volume.

We recognize that precise determination of the oscillator strength per unit volume is difficult. And so for further study, we propose to vary the loading (number) density of nanotubes for a given length. Lengths of interest of the nanotube antenna will be determined roughly by our expectations from classical antenna theory, ½ λ. As a further method of separating the electronic and optical effects, we note that, according to this model, the boron doped, nitrogen doped and pure nanotubes should each provide the same triplet interactions even though, energetically, they will have quite different positions in the HOMO-LUMO gap of the polymer host.

5.0 PROGRAM RESULTS: technology demonstrations

An important part of this research program is to provide technology demonstration platforms to more fully understand how these scientific advances can be integrated into organic electronics. The majority of our efforts in this program has been on organic photovolatics.

Photovoltaics

Approach

In this program, we have attempted to construct an ordered nanophase within polymer photovoltaics to provide dispersed nanostructured interfaces throughout the bulk of absorbing material, such that the excitons are efficiently separated into electrons and holes before recombination, and then allow for the removal of this charge (as current) in the most efficient way.

The best known nanomaterial to create such 'bulk heterojunctions' is the fullerene and its derivatives. Widely recognized as an efficient an electron acceptor a blended phase of fullerenes into a conducting organic host allows for separation of the exciton and high mobility transport of the electron. Since the hole is typically the high mobility carrier, enhancing electron mobility further serves to provide charge balance to devices. While this has worked well the hopping nature of electrons in a percolating network of fullerenes severely limits the maximum obtainable efficiency. What is needed is control over the structure of the nanophase that will allow for tailored carrier mobilities.

To control the mesophase we have attempted to create single crystalline nano-whiskers of C_{60} pointing toward the Cathode (but not touching it) from the anode. This provides an increase in the electron mobility more closely matching that of the holes in the polymer host. We demonstrate this mesophase control in the P3HT:PCBM system. In this system, P3HT is the absorber and overlaps with the solar spectrum which sets the upper limit of performance, the "Forrest Limit," at about 12%.

Test devices

The standard device used in our studies is built by spin casting PEDOT:PSS onto cleaned ITO substrates. The PEDOT:PSS layer is approximately 80 nm thick. This layer is them dried for 15 minutes at 80 °C. A blend of regioregular P3HT (Sigma Aldrich) and PCBM (American Dye Sources) is then spin coated onto the PEDOT layer and allowed to dry for 12 hours at 10^{-5} torr. Subsequently, a LiF (0.5 nm) Al cathode is evaporated onto the polymer stack. This device is removed from the evaporator and encapsulated using glass capsules with a silicon seal or our new Saran™ encapsulation (described below). Once the devices are built and encapsulated, the device is annealed on a hot plate. Performance of the devices was determined using a calibrated AM1.5G solar simulator (Oriel) at 80 mW/cm^2 illumination. Current voltage curves were obtained using a standard source measurement unit (Keithley SMU) from which the maximum power rectangle was determined. From this the filling factor and efficiency of the device was calculated.

Optimizing Performance

To optimize the device before annealing, the ratio of polymer to PCBM was determined by varying from 1:1 (polymer to PCBM) to 1:0.466 for two different thicknesses of P3HT films. Notice that the maximum efficiency was obtained at a surprisingly low loading of PCBM for both the thick (150 nm) and thin (80 nm) films shown in figure 1. Next, the optimally loaded devices were annealed (shown in figure 2a) to create ordering (crystallization) within the nanophased materials (PCBM). The devices were annealed to 150 °C for different lengths of time to determine the maximum efficiency that could be obtained. We note that lower temperatures were also investigated and it was found that 150 °C to 155 °C was the optimal annealing window to provide significant mobility to the PCBM phase. Annealing between two and three minutes results in efficiencies around 5.2 % to 5.5 %. This is an enhancement of more than 120%. We note that continued annealing at this temperature or lower, results in an overall degradation of the device performance.

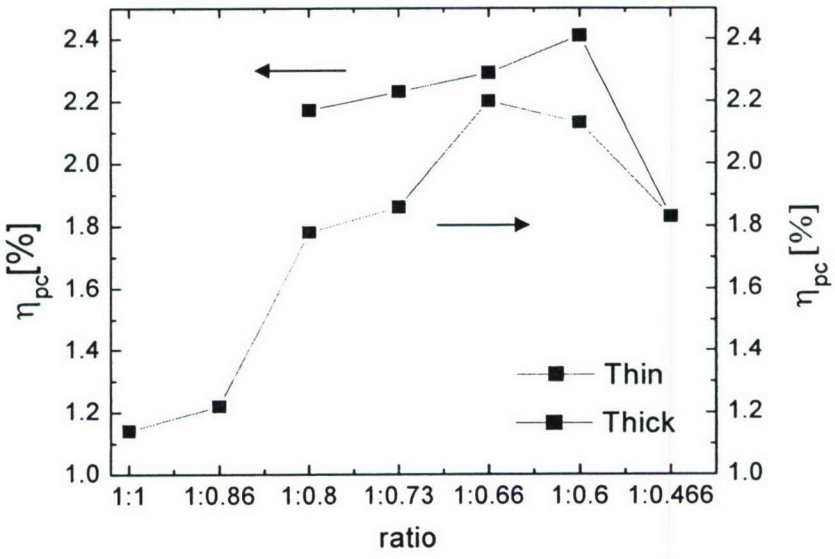

Figure 5.1: optimized performance as a function of loading before annealing for two film thicknesses

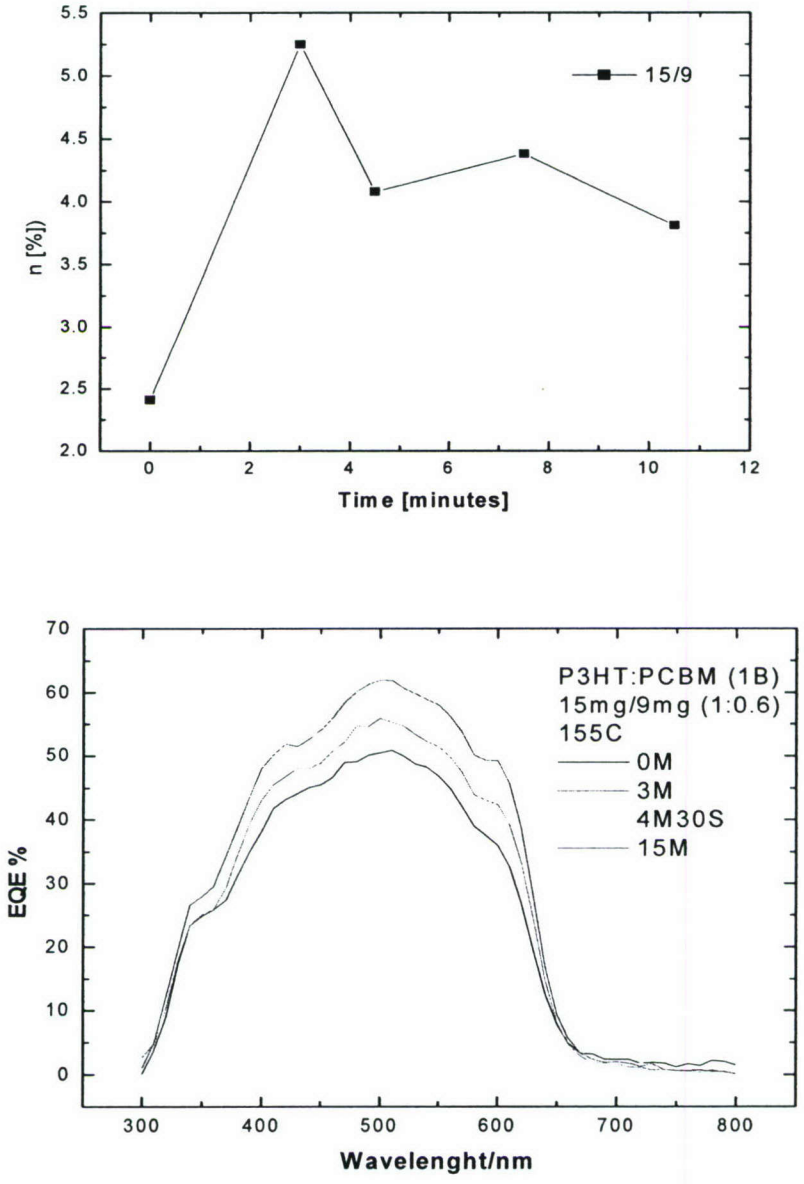

Figure 5.2: a) device efficiency after annealing process as a function of annealing times. B) EQE presented for a 1:06 ratio (polymer to PCBM) device with a 80 nm thick active layer and annealed for various times (0 minutes, 3 minutes, 4.30 minutes, and 15 minutes)

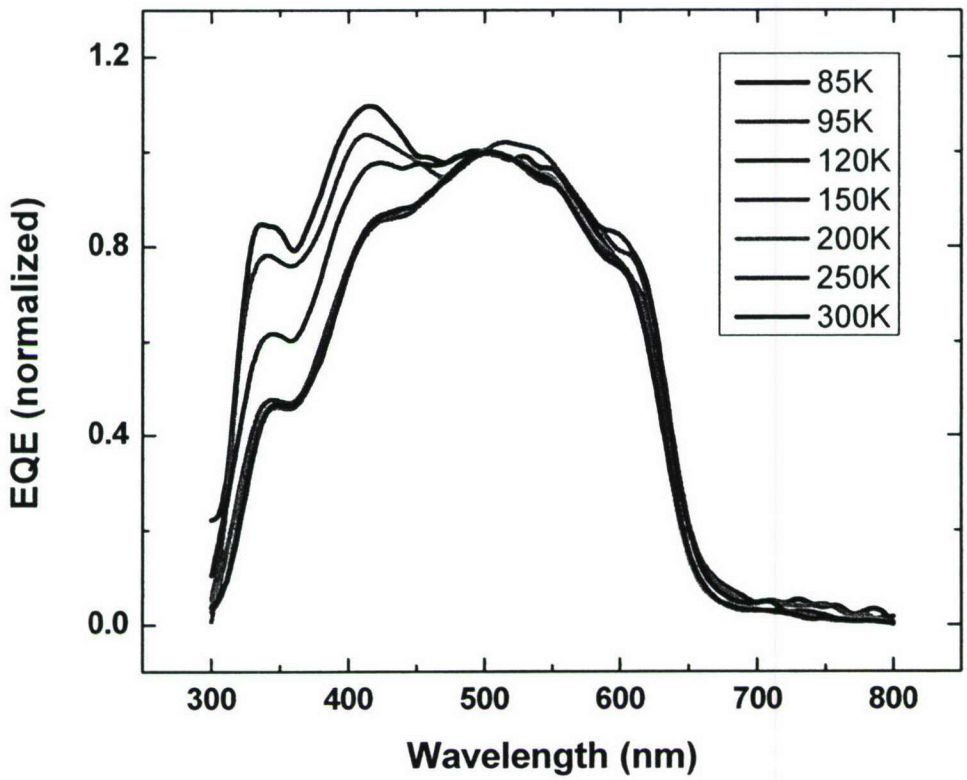

Figure 5.3: EQE for an optimally loaded and annealed device, presented as a function of temperature.

An examination of electron conduction mechanisms within the active layer shows that there is a change in the mesophase due to annealing. Shown in figure 3 is the External Quantum Efficiency (EQE) as a function of incident wavelength for temperatures between 80K and 300K (Room Temperature). Generally, the feature related to fullerene conduction of the electrons occurs at 350 nm, and the 500 nm feature is related to the polymer conduction. Notice that the fullerene feature grows rapidly compared to the polymer conduction indicating crystalline conductivity is now occurring in the mesophase. Further, relatively low hopping conductivity is seen in the fullerene component relative to the unannealed devices suggesting that the mesophase crystals extend across the P3HT layer.

The ordering of the mesophase is accompanied by a corresponding change in the absorption and luminescence of the active layer. Figure 4. compares the absorption of: PCBM, P3HT, PCBM:P3HT un-annealed blend and PCBM:P3HT annealed blend. Clearly the absorption features of the pristine materials are not reflected in a simple amalgam of the spectra from blends. The blended samples show an overall absorption red-shift as compared to their pristine states, which suggests that there is a close interaction between PCBM and P3HT. This is a consequence of the mixing of the electronic wave functions and the potential formation of a charge transfer complex (R.S. Mulliken, J.Am.Chem.Soc., 74, 811 (1952)). The peak at 3.6 eV is from PCBM, and is does not effected upon annealing. However, we can see that the P3HT absorption between 2 eV and 3 eV changes significantly. The λ_{max} which corresponds to the interband transition is red shifted by 0.02 eV to 2.45 eV, while the E_g optically calculated is also red shifted by 0.02 eV as opposed to the pristine material gap at 1.9 eV. Elsewhere, this form of blending has resulted in a blueshift as there was no ground state doping of the P3HT. The consequence of this is not that we have introduced some form of doping state, but suggests a conformational change in the packing which has made the system more packed and dense as a consequence. Changes in interchain packing or conformational changes in the polymer normally result in a blue shift for poor packing condition, while we see a red shift which is caused by tighter packing order. More significant is that the large absorption increase between 2 - 3.5 eV shows a spectral increase in absorption by 14% due to the annealing. This suggests that the device efficiency enhancement is caused in part by the increase in the overall absorption.

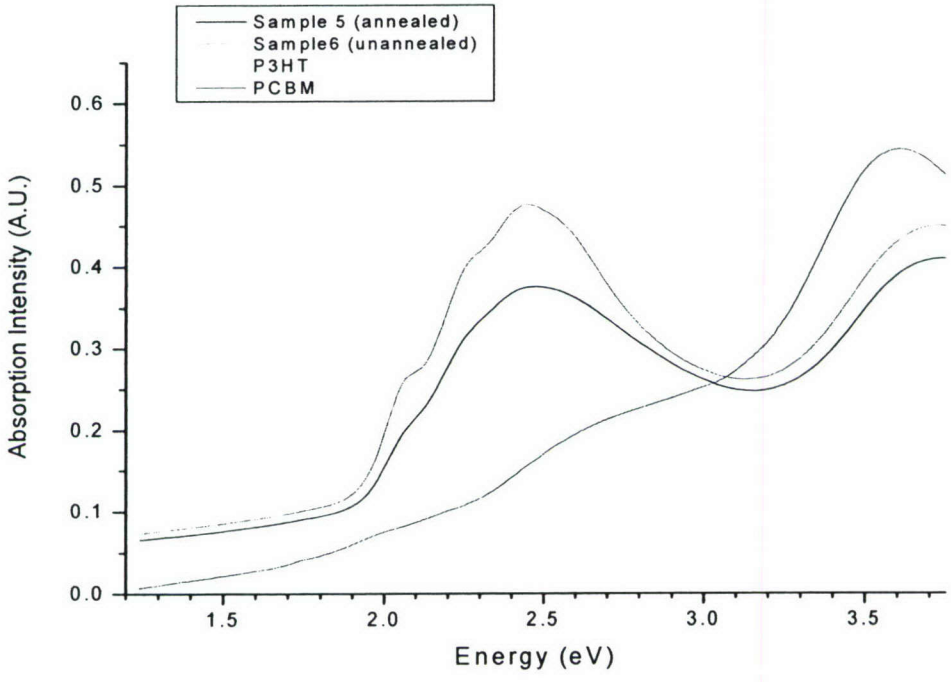

Figure 5.4: The absorption spectra of the active host before and after annealing.

Conjugated systems such as polymers will have their substantial photoluminescence quenched in the presence of C_{60}, or fullerene derivatives such as PCBM. Fluorescence spectra were obtained using a Renishaw InVia Raman spectrometer equipped with a Raman Leica RE02 microscope, the excitation source being the Ar ion laser at 457 nm. In our samples we see in Figure 5 that the PCBM fluorescence which is strongest in the infrared, is substantially quenched by being blended with PCBM. This is as expected and has been noted elsewhere and is a consequence of a charge transfer complex. In addition, there is a shift the Pl_{max} in the infrared towards the blue also indicating exciton scavenging by the PCBM. Additionally, the PCBM which fluoresces quite strongly in the infrared, has its fluorescence completely quenched. When we examine the two blended structures, while the spectra are as expected quite similar, the fluorescence is also reduced when we anneal the samples which would indicate quenching sites and enhanced exciton extraction from the more ordered and closer packed structure. However, there is a fluorescence in the P3HT from the unannealed spectrum (in the IR) and this has been even further reduced. This has to do with a greater interaction between the PCBM and its ability to enhance electron transfer due to mesophase changes.

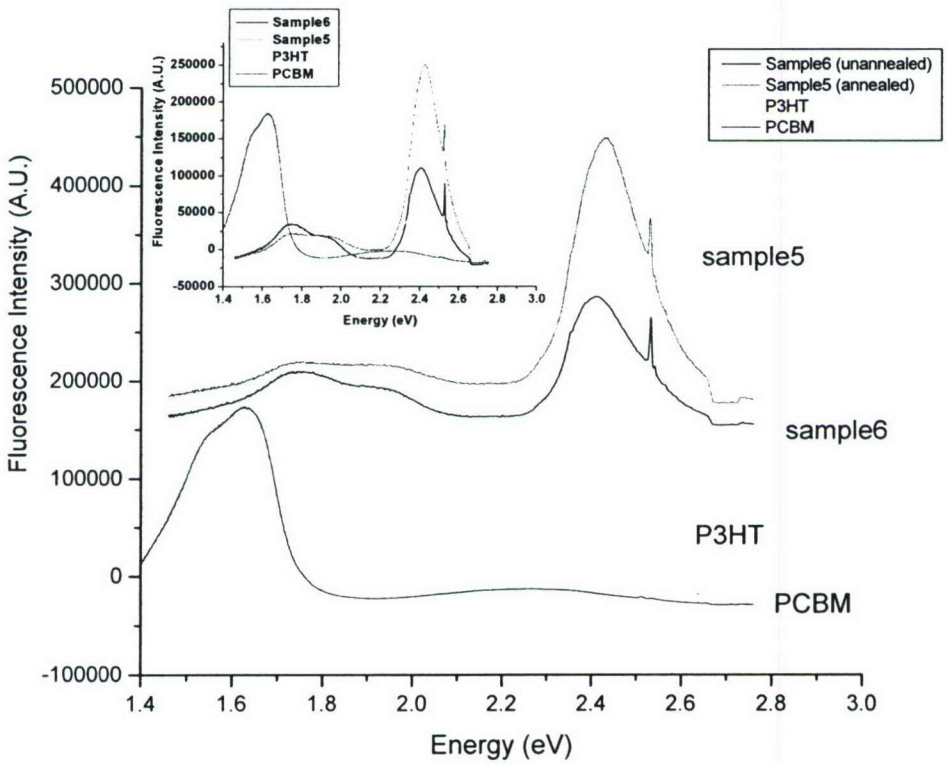

Figure 4.5: Fluorescence in the active system before and after annealing showing an enhanced quenching effect from the annealed materials (curves are offset).

This is further reflected on the nano-scale as seen in NSOM. The AFM/NSOM images shown in figure 6 were obtained using a Near-Field Scanning Optical Microscope (NSOM). This utilizes an aluminum coated optical fiber tip, mounted on a piezoelectric tuning fork which allows duel AFM/NSOM imaging. The AFM mode uses a shear force feedback method of imaging topography. Thin films of the nanocomposites were spun cast onto a glass cover, and the film was imaged using the near-field scanning optical microscope in transmission mode using a 457 nm Ar ion laser. In this way, topographical as well as optical transmission images were obtained simultaneously.

While the films are almost completely flat throughout with a variation in topography of 4 nm across a few microns, the transmission NSOM reveals more significant information on the characteristics of the mesophase. We can see that there are substantial differences in the optical transmission, as the 'spiked' structures would suggest regions of greater light transmission which would correlate to areas without the Fullerenes. In Figure 6c (annealed) and Figure 6d (unannealed) we can see changes in the optical transmission. The unannealed samples show large regions of absorption, which would suggest large aggregates of the PCBM varying in sizes from a few ten's of nm to 100's of nms. However, after annealing we see that there is a much finer detail in quenching across the film. This suggests a greater dispersion of the PCBM as the regions of little optical transition are of the order of 2-4 nm. In light of the above transport results, we interpret this as the occurrence of nano-scale crystals of PCBM. The better dispersion of PCBM nanocrystals ensures that there is a more efficient PCBM:P3HT interaction, a greater surface area for interaction, and subsequently we get better luminescence quenching with the consequence of improved exciton disassociation.

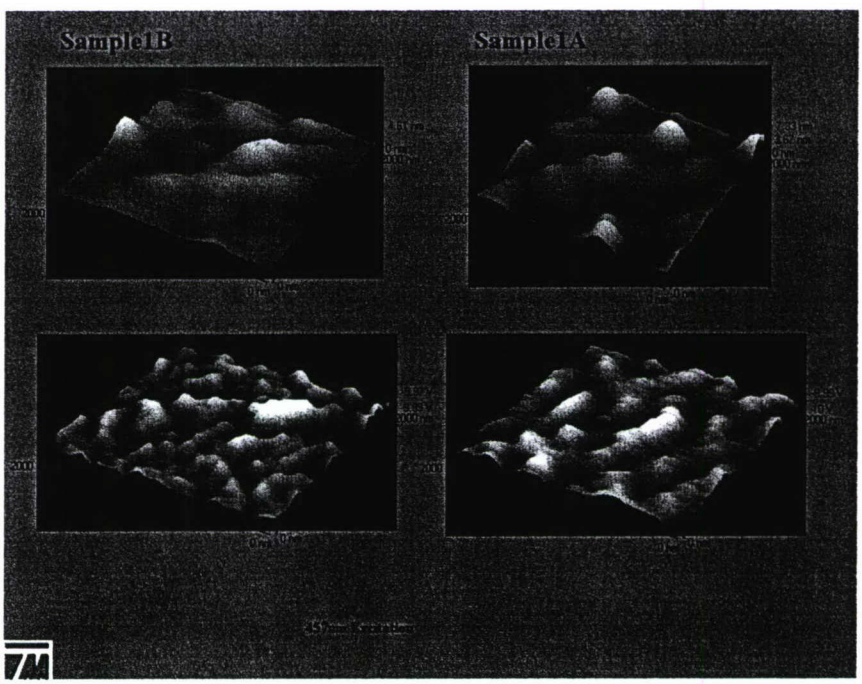

Figure 5.6: Topography of the films is shown on top. Transmission of light is shown on bottom. (1B annealed and 1A unannelaed)

Similar results have been achieved using an oriented crystal of C_{60} in the conjugated matrix where the nano-whisker is created outside of the matrix and added subsequently, thereby mitigating the necessity for annealing. Shown in Figure 7, these nano-whiskers of fullerene are created by adding purified fullerenes to an immesible blend of solvents in which the fullerene is partially soluble. In our case, Dichlorobenzene and a simple alcohol were used. The fullerene whiskers form at the interfaces of the fluids. After these are "plated" out of solution, UV polymerization was used to stabilize the whiskers and allow them to be resolubilized in DCB. The process results in whisker sizes of 100 nm long and 20 nm across. The diameter of the whisker can be controlled by use of different polymerization times.

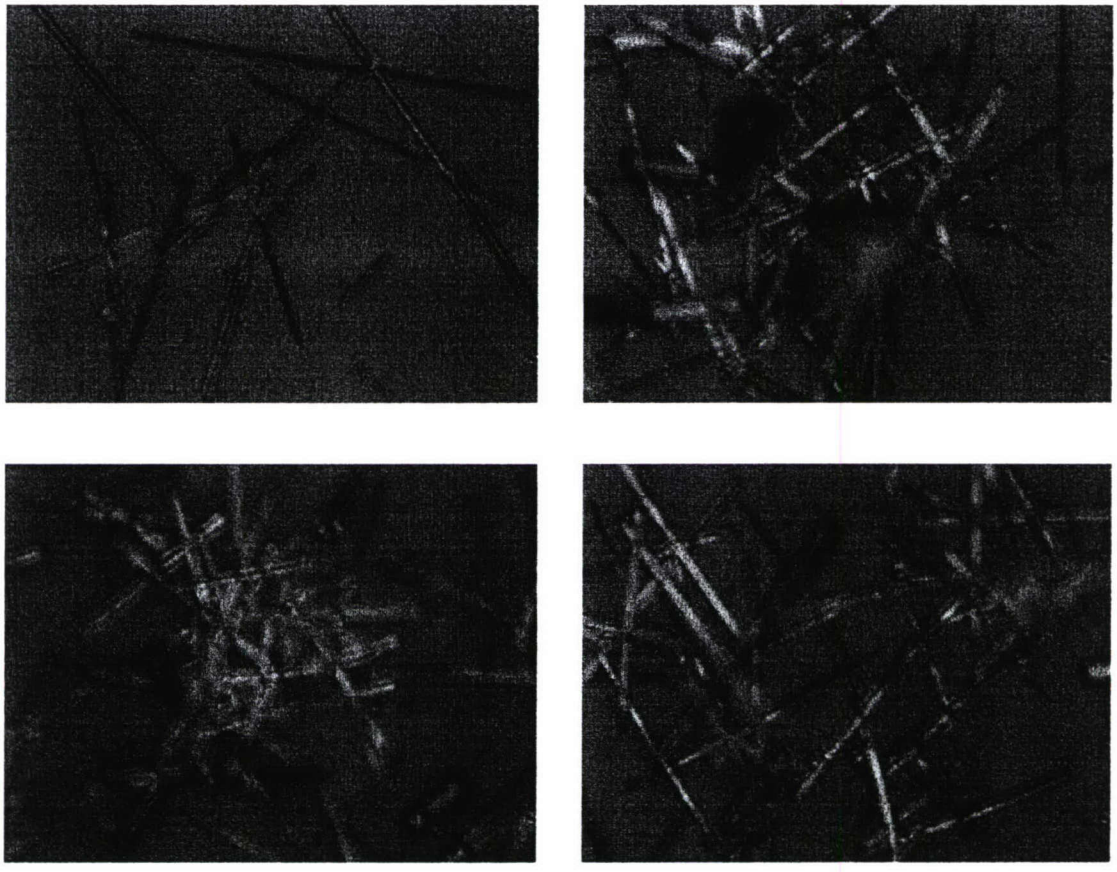

Figure 5.7: Optical micrographs of the fullerene whiskers before UV polymerization and washing. These whiskers are ~ 200 nm in diameter and microns long.

These results would tend to indicate that the overall performance of the OPV system is due to the crystalline state of the fullerene nanophase (thereby reducing hopping conduction except at the contacts) and the orientation of the whiskers within the matrix.

This report lists only the major advances of the program and is NOT exhaustive.

Naturally, the question of the form that the nanophase takes after heating has led to a number of papers since our initial announcement. We have also performed AFM and cross-sectional TEM to observe the nano-whisker crystallites as shown here.

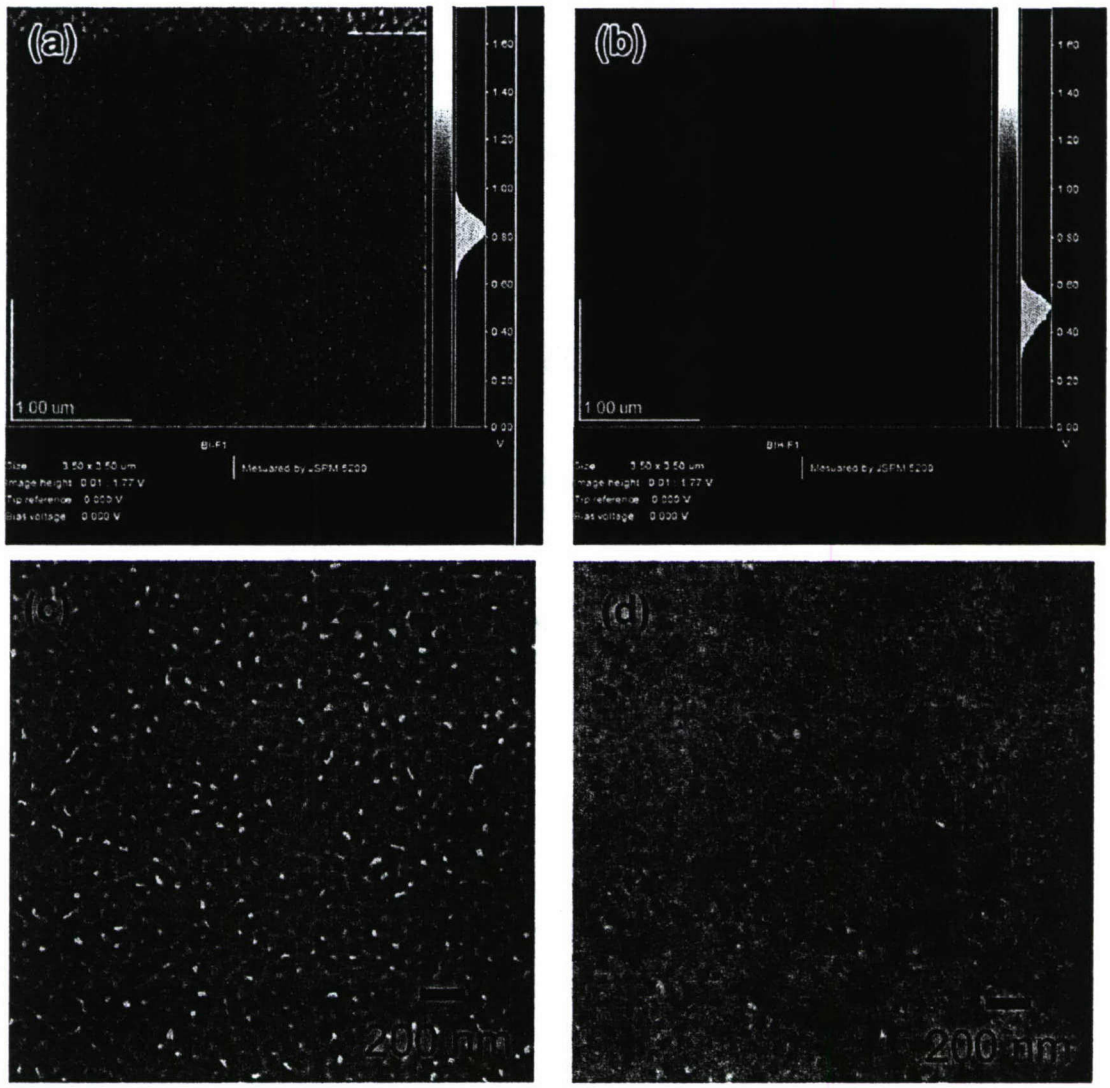

Figure 5.8: morphology of the thin film (top) AFM unannealed left, annealed right. (Below) unannealed left, annealed right.

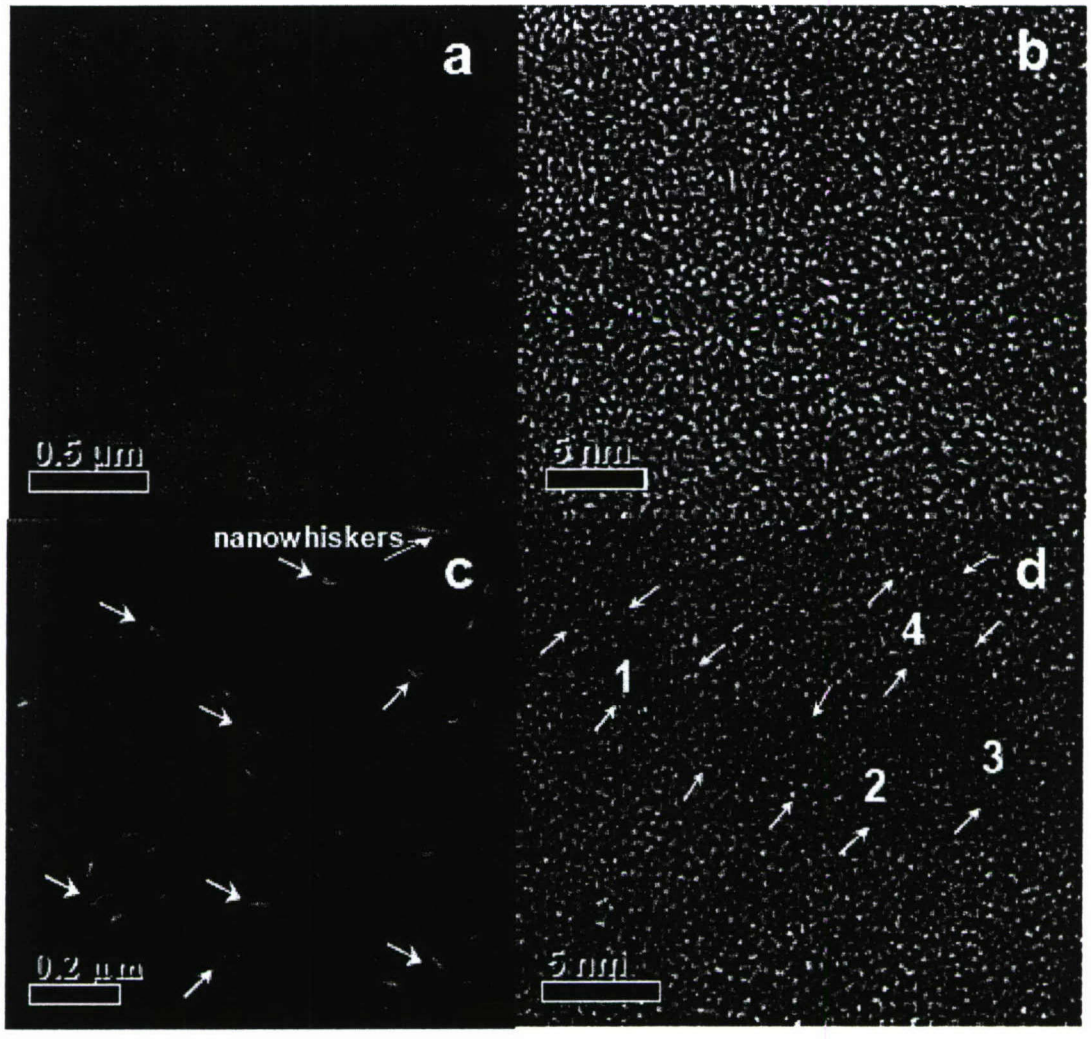

Figure 5.9: (a,c) Z-contrast and (b,d) HRTEM images of PCBM:P3HT films of 37 wt% (a,b) before and (c,d) after annealing. Elongated nanostructures are shown by arrows in (c) and (d). The numbers in the inset (f,h) show crystallized domains.

Since these whiskers appear as crystalline, then modifications to the conduction mechanisms for the electrons are also expected.

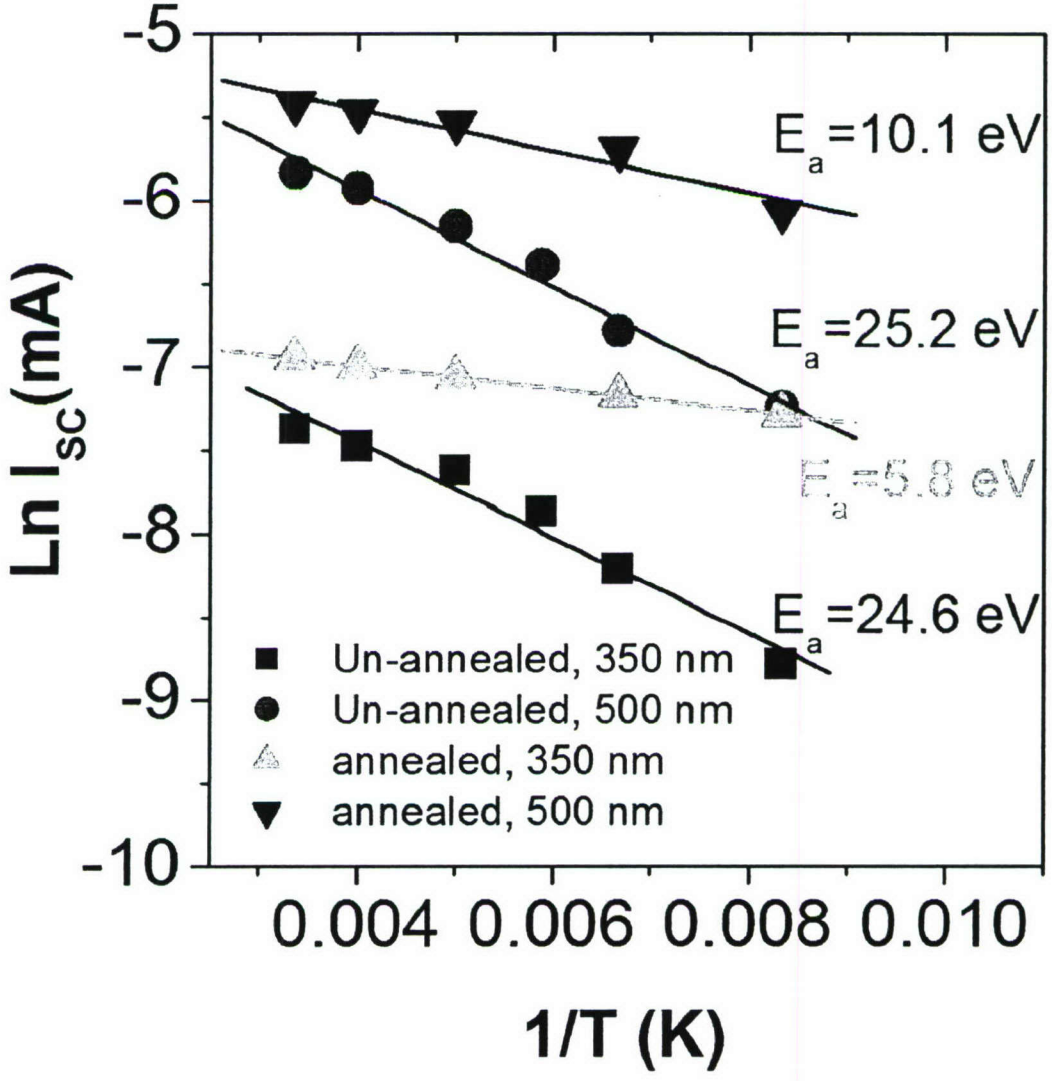

Figure 5.9: By plotting ln(Jsc) vs 1/T at specific illumination wavelengths and fitted to: $Jsc = J_0 exp(-Ea/kT)$ we can get the activation energy for transport. Notice that the current measured under 350 nm illumination (black and green above) is transport of the electrons. With annealing clearly the hopping energy decreases indicating that the overall conduction is becoming more crystalline like. This is what is expected at the whiskers appear to be becoming crystalline from the micrographs.

This report lists only the major advances of the program and is NOT exhaustive.

Metal Nanoparticles as Optical concentrators

An important aspect of device design is well established to be the overall light capturing efficiency *within* the absorption band of the active materials in the device. That is, it is important to capture ALL of the light that can be absorbed as opposed to reflecting the light away from the device. As Forrest has demonstrated, this means that the electric field strength must be greatest near the electrode such that the maximum absorption occurs in a layer ¼ of the λ of maximum absorption away from the metal anode. His approach in small molecules has been to combine organic "spacers" or multilayers, with a thin metal layer or film in the center of the device. This semi-transparent film allows for enhance near-field modes of the field to be created in the center of the device, thereby enhancing the absorption efficiency in that region of the active material.

We, following this lead, have instead added Ag and Au nanoparticles of metals freely throughout the device to better understand the effects of near-field scattering and whether phase-coherent behavior can be achieved within the absorption band of the spectrum.

Again, using the same device designs as above, based on a regio-regular poly(3-octylthiophene) (P3OT) and C_{60} blend as a donor and acceptor bulk heterojunction. Both Ag and Au nanoparticles (NP) were used as nano-phases within this active matrix. To increase the solubility, NP were stabilized with a long alkyl chain (dodecyl amine). Dodecyl amine stabilized NP are prepared as described in the literature and the size of prepared Ag and Au NP were 6.1± 1.3 and 5.3 ± 1.1 nm, respectively. The active materials were prepared by first blending P3OT (Aldrich, Mw = 87 kg mol^{-}, without further purification) and C_{60} (Aldrich) in chlorobenzene. The weight ratio of P3OT:C_{60} solution was fixed to 4:1. The concentration of P3OT:C_{60} solution was varied to achieve different film thicknesses. After preparation of P3OT:C_{60} solution, different amounts of NP were added to adjust the corresponding wt %. We considered only the P3OT weight for the determination of wt % of the NP. After preparing doped and undoped solutions, the blends were filtered with 0.2 μm PTFE syringe filter.

Figure 10(a) and (b) compares the I-V curves of Au NP "doped" and Ag NP "doped" PV devices under dark conditions, respectively. In this case, we use the language of "doping" explicitly so as to draw a correlation between the induced electronic states of the nano-phase into the HOMO-LUMO gap of the P3OT and those of dopants in semiconductors and the electronic levels in their band gaps. As shown, doping of Au or Ag NP seems to increase electrical conductivity of the film. From the graphs, the series resistance (Rs) of the P3OT:C_{60} device was calculated and shown to be reduced from 46 to 15~20 Ωcm^2. Further, the Rs value of doped device was monotonically reduced as the doping level is increased regardless of kind of nanoparticle.

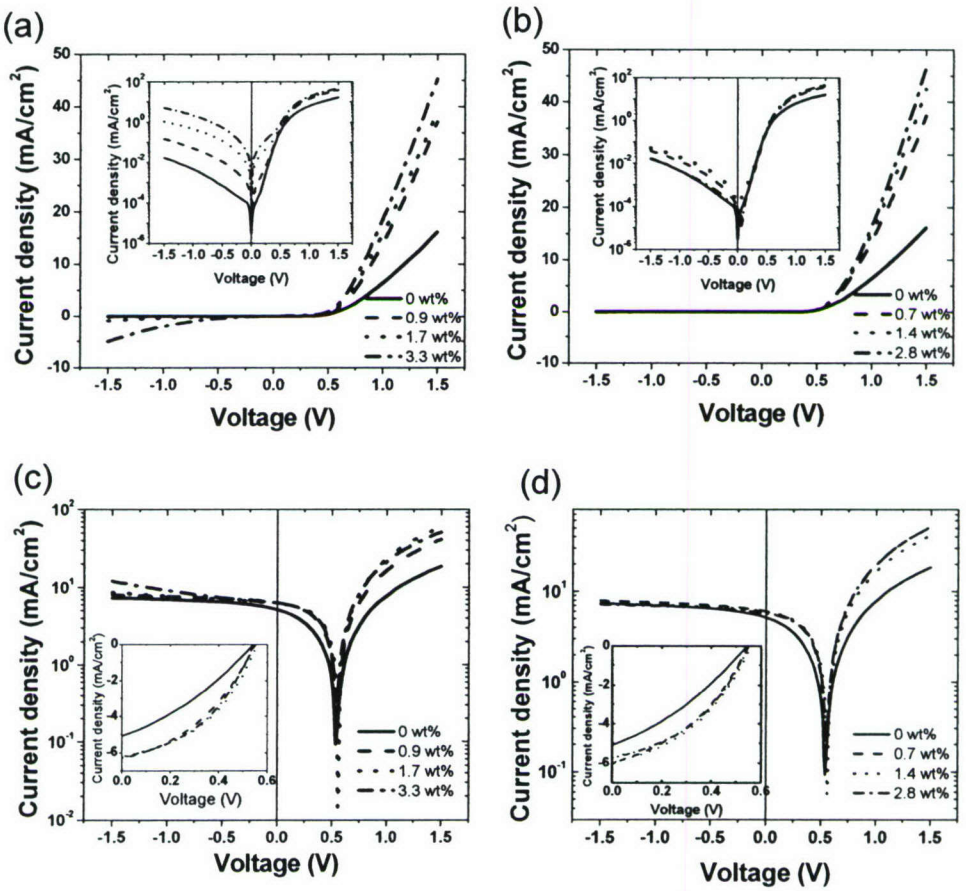

Figure 5.10: IV curves from the nano-particle doped devices with conditions as shown.

Rs calculations were done using the high voltage limit and as stated, Ag and Au doped devices are similar, indicating that the increase in conductivity is dominated by hopping conduction. However, at low voltages, before flat band conditions are met, there are striking differences between the two devices. Ag NP doped devices showed increased current density before flat band region when compared to undoped devices. The increase of current was enhanced as the doping level is increased. Au doped devices were also showed current density increase at the region but the amount was trivial when compared to Ag doped devices. Another point to be noticed is that the rectification ratio of the Ag NP doped device was reduced significantly as the doping level of NP increases. This means Ag NP doping increases the saturation current of the device. For example, the rectification ratio of an undoped device was 1000 at ± 1.5 V but at a loading of 3.3 wt%

Ag NP, a doped device has a ratio of 9. However, the ratios for the Au doped devices had values between 800 – 2000, roughly same order as that of the undoped device. Clearly, this suggests that the Ag and Au NP dopant states that occur in the band gap of the P3OT, are very different in energy. It is known that energy gap of metal nanoparticles appears at the size of ≤ 1 nm. Therefore, it is thought that NPs used in this study have bulk property of corresponding metals. If we consider the workfunctions of the Ag (4.3 – 4.7 eV) and Au (5.1 - 5.4 eV), and HOMO (4.8 – 5.2 eV) level of P3OT, we can assume that hole transfer (as a donor) from P3OT to Ag NP or electron transfer from Ag NP to P3OT is more facile than in the case of the Au NP. Thus the Au donor state sits much more deeply within the HOMO-LUMO gap of P3OT than does Ag. Further, it is known that an increase of the doping level in semiconductors increases the current density before flat band conditions[19] and the saturation current of diode devices.

Figure 10(a) and (b) represent I-V characteristics of Ag (Figure 10(c)) and Au (Figure 10(d)) NP doped PV devices under the illumination and their properties are summarized in Figure 11.

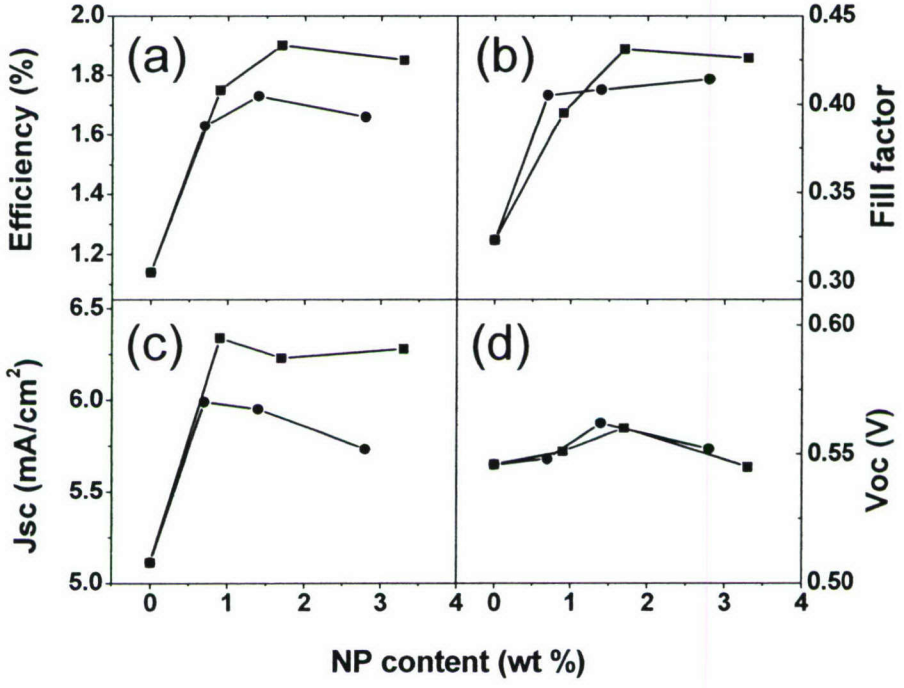

Figure 5.11: a summary of variables shown in figure 10, demonstrating effects with loading. (solid square: Ag, solid circle: Au)

The efficiency of the device was enhanced up to ~70% for Au NP and ~50% for Ag NP doping at doping level of 1.7 wt % and 1.4 wt %, respectively. There was little difference in open circuit voltage (Voc) between doped and undoped devices. Both Au and Ag doped devices showed enhanced short circuit current (Isc) and fill factor (FF). Therefore, it seems reasonable that the enhanced efficiency of NP doped devices comes primarily from increases in Isc and FF.

Recently, the Princeton group (Yakimov *et al.*) reported significant enhancements in PV device efficiency from a tandem device which has Ag nanoparticles in the middle of two photo-active layers. They found that optical intensity near the Ag NP was enhanced significantly due to scattering. As a result, absorption in the PV devices is said to have improved. We also observed increase of absorption in P3OT film by NP doping but the amount was less than 10% (as shown here in inset of figure 12(a)). Furthermore, as we can see from Figure 12(a), external quantum efficiency (EQE) spectra of undoped PV device is almost same with Au and Ag doped PV devices. We do note, however, that the concentration of our NP is far lower than those described in the Princeton study (all of the particles in the devices in that study were at a single interface yielding a large local concentration). However, from our measurements, enhanced absorption was minimal (for our blends). Yet, the overall enhancement of efficiency of our devices (1.1 -> 1.9 %) was close to that of the Princeton study (1.1 -> 2.5%). From this we suggest that the long range absorption effects in our devices do not seem to be an important factor. As we described above, it is clear that incorporation of highly conducting Au and Ag NP helps to increase the electrical conductivity of the PV device and this seems to be the major contributor to performance enhancement. If a device's electrical conductivity is increased, more photo-generated charge carriers reach the electrode without recombination, which leads to Isc increase. Also, it is well known that FF is closely related to Rs of the PV device. A slight increase of Rs reduces FF significantly and, as a result, the power conversion efficiency will be reduced significantly. In our device, the FF of undoped device (0.32) was increased to 0.43 and 0.41 by Ag and Au doping, respectively. Those are considerable increases and will enhance the efficiency. This electrical conductivity improvement with NP doping enables us to built thicker devices. One of critical problems in organic PV devices is thinness of the active layer, necessary due to migration length of the excitons (low carrier mobility). Therefore, the device will not absorb light efficiently. (This is the purpose of using the scattering layer in the Princeton study). We note, however, that the NP doped devices showed maximum efficiency for thicker active layers. As shown in Figure 10(b), the maximum efficiency of Au doped PV device is obtained at the film thickness of ~150 nm, whereas the efficiency of undoped PV devices start to decrease after ~100 nm. This further supports the idea that the overall enhancement of performance derives from an increase in active layer mobility. Further, the maximum obtainable performance depends on the exact position within the HOMO-LUMO gap of the NP induced electronic state. That is the overall hopping energy between particles plays an important role in the internal resistance of the device. This is suggested because we find for low loading levels of NP, the Ag NP out perform the Au NP. We note that even though the plasmon absorptions of the two

particles are different (λ_{max} = 443 nm for Ag NP, and 523 nm for Au NP), the loading levels are fairly low and there is little difference between overall shape of the absorption

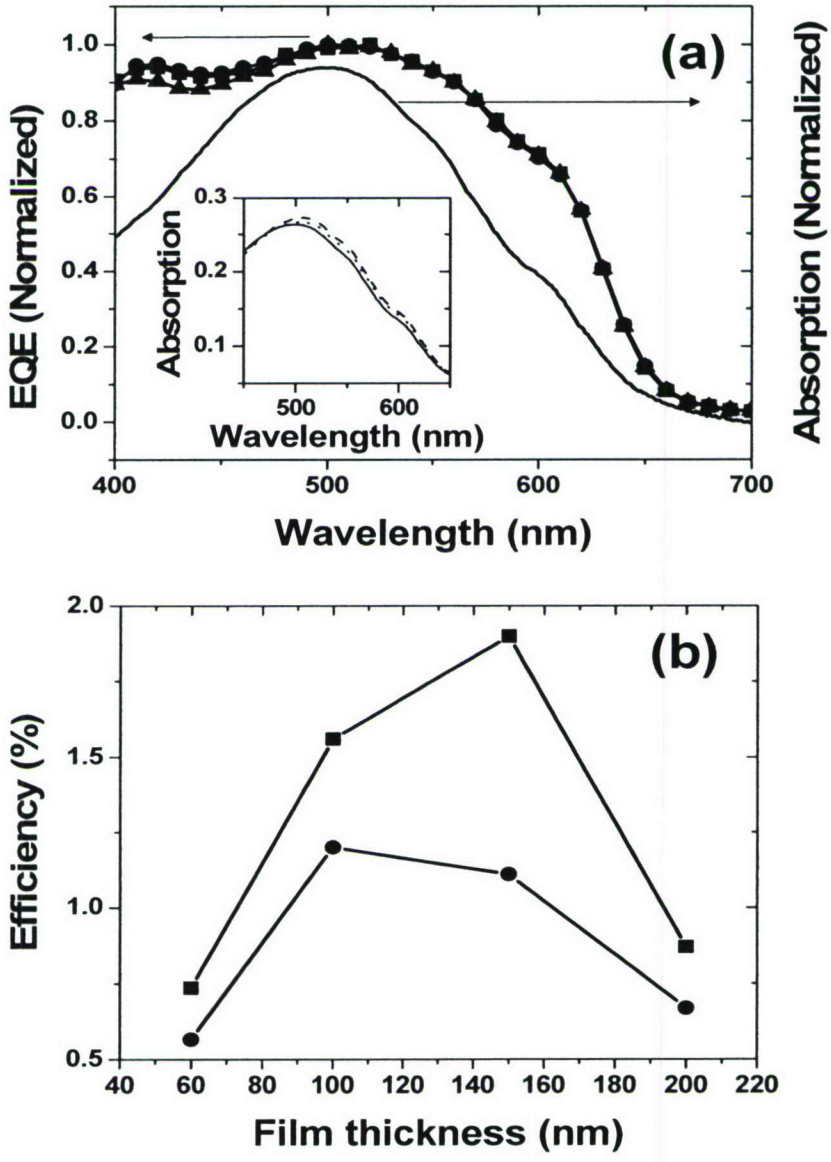

of the active layer with either Au NP and Ag NP dopants as shown in inset of figure 12(a).

Figure 5.12: Comparisons between Ag and Au performance as nano-concentrators in standard OPV devices.

Summary

Through optimization of the above considerations the highest performance we have achieved has been 6.1 % in PCE. This astonishing improvement in performance has been achieved solely through the understanding and insight gained in the program through a careful study of charge transfer and energy partitioning in a controlled and ordered meso-morphology.

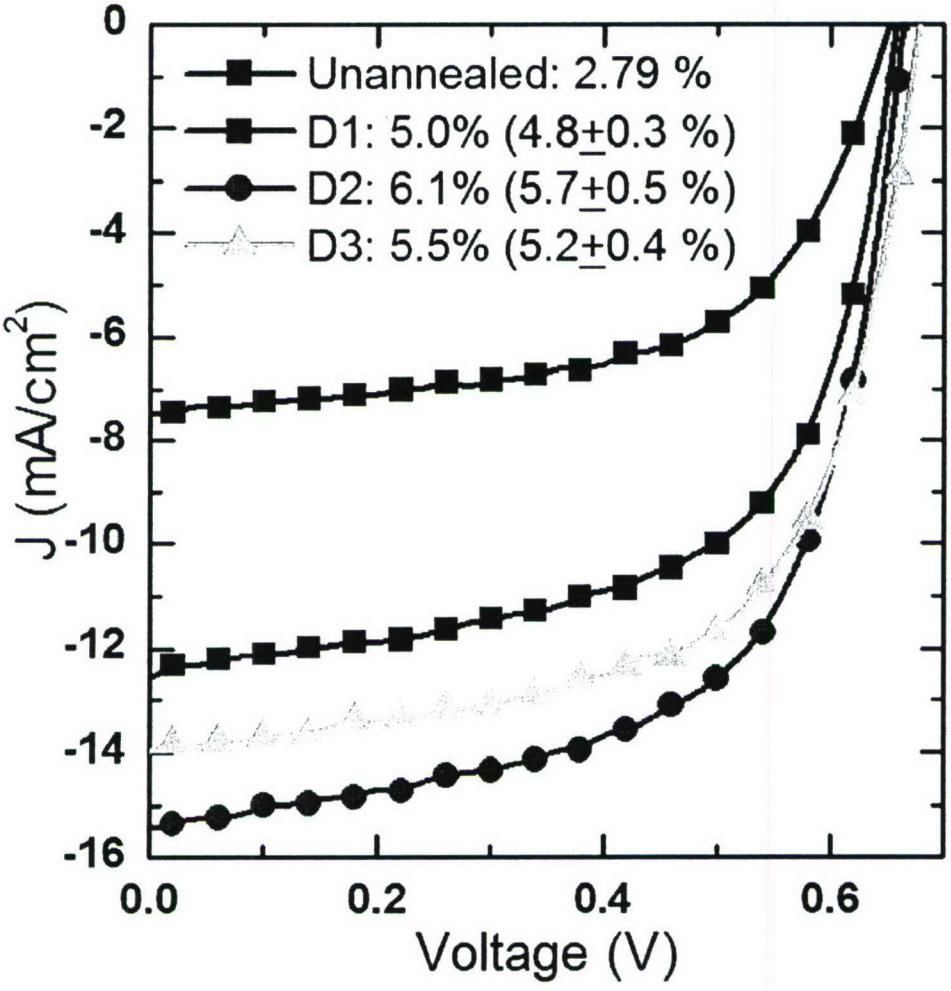

Figure 5.13. The I-V characteristics of P3HT:PCBM BHJ PV with different P3HT:PCBM film thickness. The inset legend gives the efficiencies of the data graphs

shown. The average over several devices is given in parenthesis with the mean variation. The active, or absorbing layers in D1 devices were 120 nm thick, D2 devices were 150 nm thick, and D3 devices were 180 nm thick.

This composite technology has now been integrated into a fiber based optical geometry for the possible extension of performance through optical engineering. Poly(3-hexylthiophene):1-(3-methoxycarbonyl)-propyl-1-phenyl-(6,6)C_{61} (P3HT: PCBM) photovoltaic devices were fabricated as a cladding onto large diameter optical fibers. The measured short circuit current density (J_{sc}), open circuit voltage (V_{oc}), and power conversion efficiency (η) of the devices were dependent on fiber diameter as well as the angle of incidence of light onto the cleaved fiber face. This suggests that absorption by the active layer is dominated by different mechanisms at different angles: evanescent coupling of the light at small incident angles and far field scattering of the light from the fiber at higher angles. The basic structure of the system is shown below.

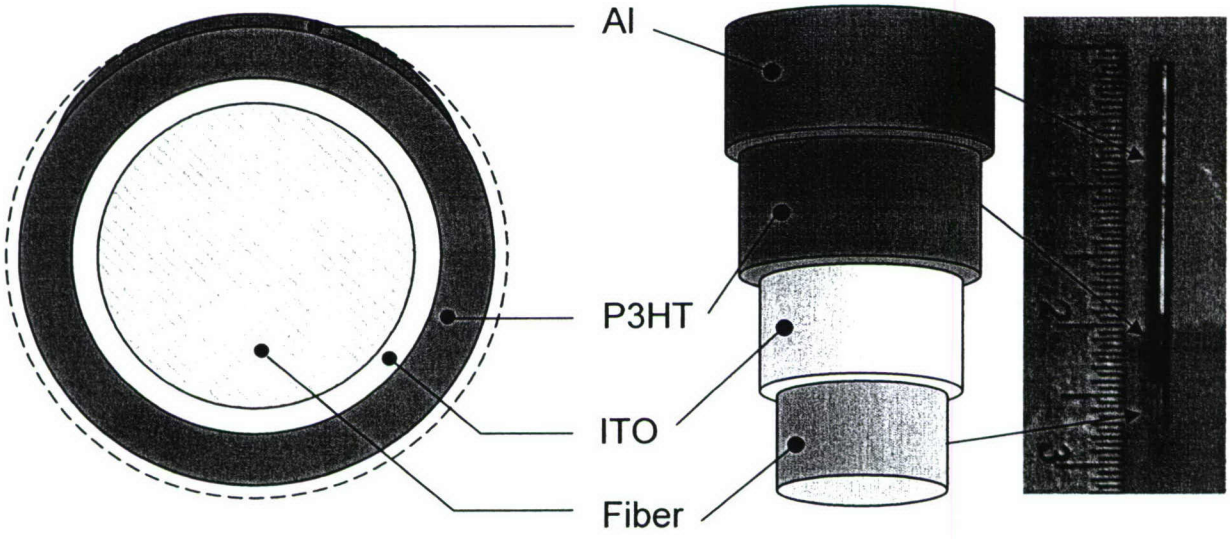

Figure 5.14: The outer contact can be fully cladded, or only partially. When the outer metal coating covers only 1/3 of the fiber, the modes of radiation are not confined and this shows up in the performance.

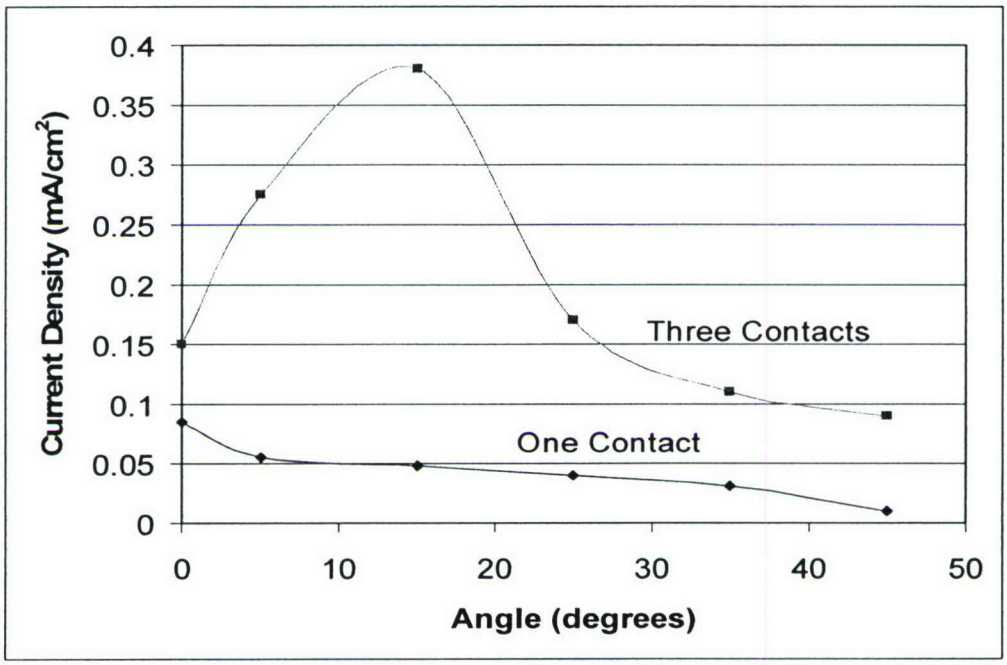

Figure 5.15; the current density jumps dramatically in a 1.5 mm DIA optical fibercell when three contacts are used for any angle of incident radiation coupling into the device.

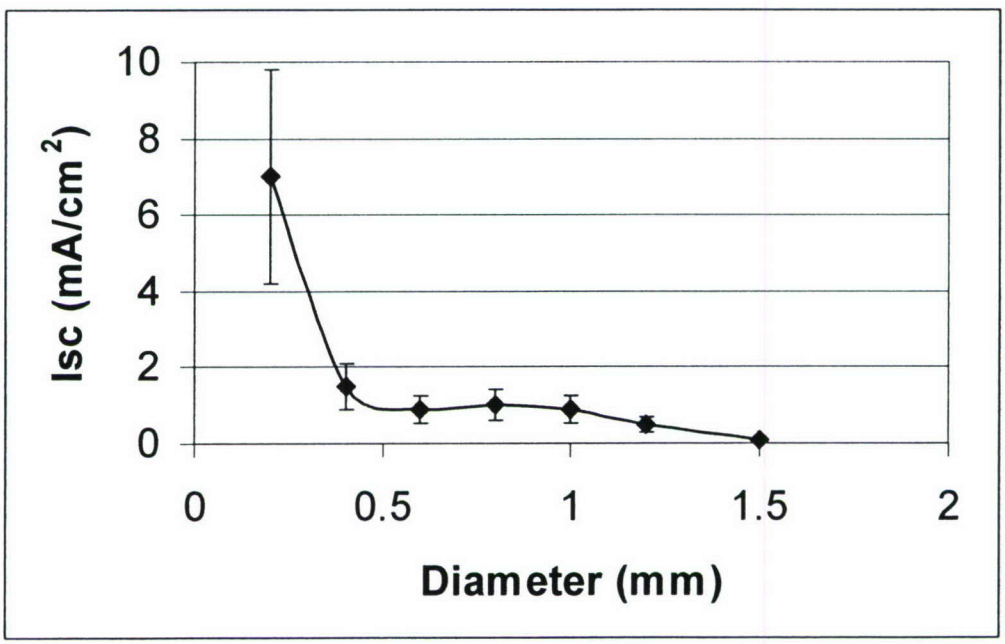

Figure 5.16: As the DIA of the optical fiber is reduced, loss into the cladding increases, thereby increasing the overall performance of the device. Shown here are the current densities of one contact devices. They correspond to a max. performance exceeding 6 % for a 0.2 mm DIA fiber. 0.1 mm fibers are projected to near 12 %.

This report lists only the major advances of the program and is NOT exhaustive.

6.0 STATS

Personnel Supported:

Ms. Faith Coldren	½ student	microscopy
Dr. Reyes-Reyes	½ time postdoc	Device building
Mr. Scott Webster	student	optical metrology
Dr. David L. Carroll	PI	
Dr. Kyung Kon Kim	Postdoc Associate	photonic crystals
Dr. Jiwen Liu	Postdoc Associate	Devices
Dr. Manoj Namboothiry	Postdoc Associate	Devices

Papers:

1. Nicole Levi, Richard Czerw, Shuya Xing, Preethi Iyer, and David L. Carroll, "Properties of Polyvinylidene Difluoride-Carbon Nanotube Blends" NANO LETTERS, 4 (7): 1267-1271 JUL 2004
2. Sihai Chen, and David L. Carroll, "Silver Nanoplates: Size Control in Two Dimensions and Formation Mechanisms," *J. Phys. Chem. B* 2004, *108,* 5500-5506
3. R. Czerw, D. L. Carroll, H. S. Woo and Y. B. Kim, and J. W. Park "Nanoscale observation of failures in organic light-emitting diodes" Journal of Applied Physics Vol. 96, No. 1, 2004 641 – 644.
4. Carroll, DL; Czerw, R; Webster, S, Polymer-nanotube composites for transparent, conducting thin films, *SYNTHETIC METALS*, 155 (3): 694-697 DEC 15 2005
5. S. Webster, R. G. Grant, R. Czerw, J. Liu, M. Terrones, N. Grobert, and D. L. Carroll, "Investigation of Iron filled Nitrogen Doped Carbon Nanotubes" *New Journal of Physics* 6, Art. 031, 2004
6. Sihai Chen, S. Webster, R. Czerw, Jianfeng Xu, and D. L. Carroll "Morphology Effects on the Optical Properties of Silver Nanoparticles" *Journal of Nanoscience and Nanotechnology* 4(3) 2004, 254-259..
7. S. Webster, R. Czerw, R. Nesper, J. DiMaio, J.-F. Xu , J. Ballato, and D. L. Carroll, "Optical Properties of Vanadium Oxide Nanotubes" *Journal of Nanoscience and Nanotechnology* 4(3) 2004, 60 – 64.
8. J. Xu, M. Xiao, R. Czerw, and D.L. Carroll, "Optical limiting and Enhanced Optical Nonlinearity in Doped Carbon Nanotubes," Chem. Phys. Lett. 389, 2004, 247-250.
9. Scott Webster, Marisol Reyes-Reyes, Xavier Pedron, Román López-Sandoval, Mauricio Terrones, and David L. Carroll, "Enhanced Nonlinear Transmittance by Cooperative Nonlinear Mechanisms: a reverse saturable absorbing carbocyanine dye blended with nonlinear scattering carbon nanotubes" Advanced Materials Volume 17, Issue 10, May, 2005, Pages: 1239-1243 (2005)
10. Kyungkon Kim, Scott Webster, Nicole Levi, Mauricio R. Pinto, Kirk S. Schanze, and David. L. Carroll, Luminescent Poly(phenylene ethynylene) Coated Silica Opals, 21(11) Langmuir, pp 5207 - 5211 (2005)
11. Hua Bao, George Chumanov, Richard Czerw, David L. Carroll, Stephen H. Foulger; Colloid Polym Sci (2005) 283: 653–661.
12. Woo HS, Kim YB, Czerw R, Carroll DL, Ballato J, Ajayan PM; Tailoring hole transport in organic light-emitting devices using carbon nanotube-polymer nanocomposites Journal of The Korean Physical Society (2004) 45 (2): 507-511.
13. Kyungkon Kim and David L. Carroll, Roles of Au and Ag Nanoparticles in Efficiency Enhancement of Poly(3-octylthiophene) / C60 Bulk Heterojunction Photovoltaic Devices, Applied Physics Letters, 87, 203113 (2005).

This report lists only the major advances of the program and is NOT exhaustive.

14. Marisol Reyes-Reyes, Kyungkon Kim, David L. Carroll, High Efficiency Photovoltaic Devices based on Annealed Poly(3-hexylthiophene) and 1-(3-methoxycarbonyl)-propyl-1-phenyl-(6,6)C61 Blends, Appl. Phys. Lett. 87, 083506 (2005)
15. Curran, SA; Talla, JA; Zhang, D; Carroll, DL, Defect-induced vibrational response of multi-walled carbon nanotubes using resonance Raman spectroscopy, *JOURNAL OF MATERIALS RESEARCH*, 20 (12): 3368-3373 DEC 2005
16. J. Liu and D.L. Carroll, Temperature and Flow Rate of NH3 Effects on Nitrogen Content and Doping Environments of Carbon Nanotubes Grown by Injection CVD Method, J. Phys. Chem. B.; (Article); 2005; 109(33); 15769-15774
17. B. Berzina, L. Trinkler , R. Krutohvostov, R. T. Williams , D. L. Carroll, R. Czerw, E. Shishonok , Photoluminescence excitation spectroscopy in boron nitride nanotubes compared to microcrystalline h-BN and c-BN, physica status solidi (c) Volume 2, Issue 1 , Pages 318 – 321 (2005)
18. Reyes-Reyes, M.; Kim, K.; Dewald, J.; Lopez-Sandoval, R.; Avadhanula, A.; Curran, S.; Carroll, D.L., Meso-Structure Formation for Enhanced Organic Photovoltaic Cells, Org. Lett.; 2005; 7(26); 5749-5752.
19. Liu, J; Czerw, R; Carroll, DL, Large-scale synthesis of highly aligned nitrogen doped carbon nanotubes by injection chemical vapor deposition methods *JOURNAL OF MATERIALS RESEARCH*, 20 (2): 538-543 FEB 2005
20. Woo, HS; Cho, S; Kwon, TW; Park, DK; Kim, YB; Czerw, R; Carroll, DL; Park, JW, Truly blue organic light-emitting diodes based on carbazole-doped 4,4 '-Bis[carbazolyl-(9)]-stilbene, *JOURNAL OF THE KOREAN PHYSICAL SOCIETY*, 46 (4): 981-984 APR 2005
21. Kyong Kon Kim, Jiwen Liu, and D.L. Carroll, Thermal Diffusion Processes in Bulk Heterojunction Formation for Poly-3-hexylthiophene / C60 Single Heterojunction Photovoltaics, Appl. Phys. Lett. 88, 181911 (2006)
22. D.L. Carroll, Polymer solar cells achieve 5.2% efficiency, LASER FOCUS WORLD, 42 (2): 11-11 FEB 2006.
23. J. Liu, S. Webster and D.L. Carroll, Highly Aligned Helical Nitrogen Doped Carbon Nanotubes Synthesized by Injection Assisted Chemical Vapor Deposition, Appl. Phys. Lett. 88, 213119 (2006).
24. A. G Manoj, T. Zimmerman, F. M. Coldren, J. Liu, K. Kim, D. L. Carroll, "Electrochromic Properties of Conducting Polymer Metal Nanoparticles Composites" Submitted to Synthetic Metals (2006).
25. D. L. Carroll, R. Czerw, and B. S. Harrison, "Carbon Nanotube – Poly 3-octylthiophene Composite Photovoltaic Cells" J. Nanosci. Nanotechnol. 6, 2204–2207 (2006)
26. B. Berzina, L. Trinkler, V. Korsak, R. Krutohvostov, D. L. Carroll, K. B. Ucer and R. T. Williams, Exciton luminescence of boron nitride nanotubes and nano-arches Physica Status Solidi (b) Vol. 243/14/2006, page 3840-3845
27. Nicole Levi, Roy R Hantgan, Mark O Lively, David L Carroll, Gaddamanugu L Prasad, C_{60}-Fullerenes: detection of intracellular photoluminescence and lack of cytotoxic effects, Journal of Nanobiotechnology 2006, 4:14 (14 December 2006)
28. F.-X. Zha, S. Roth and D.L. Carroll, Periodic, pearl chain-like nanostructure observed by scanning tunneling microscopy, Carbon, Volume 44, Issue 9, August Pages 1695-1698 (2006)
29. Vieira SMC, Stephan O, Carroll DL, Effect of growth conditions on B-doped carbon nanotubes, JOURNAL OF MATERIALS RESEARCH 21 (12): 3058-3064 DEC 2006
30. Curran S, Dewald J, Carroll DL, All-optical nanoscale read/write bit formation, JOURNAL OF MICROLITHOGRAPHY MICROFABRICATION AND MICROSYSTEMS 5 (1): Art. No. 011013 JAN-MAR 2006
31. Liu J, Carroll DL, Cech J, Roth S, Single-walled carbon nanotubes synthesized by the pyrolysis of pyridine over catalysts, JOURNAL OF MATERIALS RESEARCH 21 (11): 2835-2840 NOV 2006
32. Curran SA, Zhang DH, Wondmagegn WT, Ellis AV, Cech J, Roth S, Carroll DL, Dynamic electrical properties of polymer-carbon nanotube composites: Enhancement through covalent bonding, JOURNAL OF MATERIALS RESEARCH 21 (4): 1071-1077 APR 2006

This report lists only the major advances of the program and is NOT exhaustive.

33. Jiwen Liu, Manoj A. G. Namboothiry, and David L. Carroll, Fiber-based architectures for organic photovoltaics Appl. Phys. Lett. 90, 063501 (2007
34. Jiwen Liu, Manoj A. G. Namboothiry, and David L. Carroll, Optical geometries for fiber-based organic photovoltaics Appl. Phys. Lett. 90, 133515 (2007) (reprinted in the Virtual Journal of NanoSciences)
35. Kyong Kon Kim, Jiwen Liu, Manoj Namboothiry, David L. Carroll, The roles of donor and acceptor nanodomains in 6% efficient thermally annealed photovoltaic devices, Accepted in APL.
36. R. T. Williams, K. B. Ucer, D. L. Carroll, B. Berzina, L. Trinkler, V. Korsak, R. Krutohvostov, Photoluminescence of self-trapped excitons in boron nitride nanotubes, submitted to JNN (2006)
37. Scott Webster*, Richard Williams, David L. Carroll, Enhanced Absorption in a Reverse Saturable Dye Blended with Carbon Nanotubes, accepted to JNN (2006)
38. Suzy V. Torti, Fiona Byrne, Orla Whelan, Nicole Levi, Burak Ucer, Michael Schmid, Frank M. Torti, Steven Akman, Jiwen Liu, Pulickel M. Ajayan, Omkaram Nalamasu and David L. Carroll "Photo-dynamic Therapeutics based on CNx Multi-Walled Nanotubes" accepted International Journal of Nanomedicine
39. R Jayakanth, A G Manoj, J Liu, I Manna and D L Carroll, "A Novel Polymer Nanotube Composite for Photovoltaic Packaging Applications" Submitted to Synthetic Metals (2006)
40. J.E. Kielbasa, J. Liu, K.B. Ucer, D.L. Carroll, and R.T. Williams, "Sol-gel nanocomposites as metamaterials: preparation and optical measurements" accepted Journal of Materials Science: Materials in Electronics
41. M. Reyes-Reyes, R. López-Sandoval, J. Liu, and D.L. Carroll "Bulk heterojunction organic photovoltaic based on polythiophene-polyelectrolyte carbon nanotube composites", Thin Solid Films (2007)
42. Benjamin S. Harrison, David Rickard, Wenhua Liu, Martin Guthold, and David L. Carroll Enhanced Conductivity of PEDOT-PSS Blended with Non-conductive Polymers and Single-walled Carbon Nanotubes, Polymer Preprints (American Chemical Society, Division of Polymer Chemistry) 45, no. 1 (2004): 153.
43. Sihai Chen and David L. Carroll, Controlling 2-Dimensional Growth of Silver Nanoplates, Self-Assembled Nanostructured Materials Editors: Yunfeng Lu, C. Jeffrey Brinker, Markus Antonietti, Chunli Bai, MRS Proceedings Volume 775 (2004)

Invited lectures at international meetings:

1. International Workshop on Conjugated Polymers "Carbon Nanotube Cancer Therapeutics" Wollongong Australia (Feb 2007)

2. International Workshop on Conjugated Polymers "High efficiency photovoltaics" Wollongong Australia (Feb. 2007)

3. International Conference on Defects in Materials (ICDIM) "Negative Index Materials" Prague Czech Republic (June 2006)

4. International Conference on Synthetic Metals "High efficiency Solar Cells" Dublin Ireland (June 2006)

5. International Winter School "High Efficiency Solar Cells" Kirchberg Austria (March 2006)

6. Optical Society of America "High Efficiency Solar Cells" Uncasville (CT) (April 2006)

7. American Chemical Society (Colloid Section) "Colloidal Crystals with Conjugated Systems" Potsdam, NY (June 2005)

8. Int. Conf. on Quantum Transport and Quantum Functional Materials "Advances in Organic Device Technologies" Bologna, Italy (June 2005)

This report lists only the major advances of the program and is NOT exhaustive.

9. American Chemical Society "Applications of Iron Filled Nanotubes" San Diego, CA (April 2005)

10. International Conference on Synthetic Metals "Advances in nanocomposite based devices" Wollongong, Australia (June 2004)

11. American Physical society Regional Meeting "Advances in Organic Device Physics" Oak Ridge TN (Nov 2004)

12. Optical Society of America, Optics in the Southeast "Optical limiting in carbon nanotubes and their variants" Charlotte, NC (Nov. 2004)

13. Nanotec' 04 "Advances in nanocomposite-based devices" Batz-Sur-Mer, France (Aug 2004)

14. ISOPL (International Society for Optical Power Limiting) "Optical Limiting in Carbon Nanotubes: Materials Modifications" Tucson, Az. (April 2004)

Patents:

D. Carroll, Manoj Namboothiry, Jiwen Liu, "Organic optoelectronic devices and applications thereof" (PCT filed May 1, 2006)

D. Carroll, Nicole Levi, Faith Coldren, "Methods and compositions for printing biologically compatible nanotube composites" (Provisional filed April 2006)

D. Carroll, S. Curran, "Fiber photovoltaic devices and applications thereof" (Provisional filed May 1, 2006)

D.L. Carroll, S. Akman, F. Torti, S. Torti, O. Nakasuma, P.M. Ajayan, "Novel carbon nanostructures for cancer therapeutics" (Provisional filed May 2006)

D. Carroll, Nicole Levi, Faith Coldren, Manoj Namboothiry, Larry Webb, Thomas Smith, William Wagner, "Novel Nano-Scale pressure sensors" (provisional filed Jan. 2006)

D. Carroll, Nicole Levi, John Stewart, "Novel Oxilaplatin delivery mechanisms for Cancer therapeutics" (Disclosure filed May 2006)

D. Carroll, Manoj Namboothiry, Jiwen Liu, "Nanocomposite lighting system" (provisional filed 2006)

D Carroll, Manoj Namboothiry, Jiwen Liu, "Thermal treatment of thin film photovoltaics" (provisional filed 2006)

(all list AFOSR funding)

This report lists only the major advances of the program and is NOT exhaustive.

Transitions:

Carroll, Wake Forest University, b. nanoparticles for Surfaced Enhanced Raman, c. Transition to David Rauh, EIC Corp Waltham MA, d. Testing for possible insertion in hand-held bio-sensor.

Carroll, Wake Forest University, b. nanocomposites for OLEDs c. Transition to Yazaki Meter Corporation Susono City Japan, d. Testing for possible insertion into dashboard displays. (This transition possibility consists of assignment of IP rights).

Carroll, Wake Forest University, b. nanocomposites for solid state lighting c. Transition to Daryl Beaudreux Nanoholdings Inc NJ, d. licensing for company startup.

Carroll, Wake Forest University, b. fibercell technologies for advanced organic photovoltaics c. Transition to Daryl Beaudreux Nanoholdings Inc NJ, d. licensing for company startup.

Carroll, Wake Forest University, b. ordered nanocomposites for photovoltaics c. Transition to Konarka Inc Lowell MA, d. testing for possible licensing opportunities.

Carroll, Wake Forest University, b. ordered nanocomposites for photovoltaics c. Transition to Plextronics Inc Pittsburg PA, d. testing for possible licensing opportunities.

END